

# Chapter 9

## Optical Properties

**Abstract** After introduction of the complex dielectric function, reflection, diffraction are briefly discussed. The focus lies on absorption mechanisms; several transition types (direct and indirect band-band transitions, impurity-related transitions, lattice absorption) are discussed including the effects of excitons, polaritons and high carrier density. Also the various effects of the presence of free carriers are given.

### 9.1 Spectral Regions and Overview

The interaction of semiconductors with light is of decisive importance for photonic and optoelectronic devices as well as for the characterization of semiconductor properties. When light hits a semiconductor, reflection, transmission and absorption are considered, as for any dielectric material. The response of the semiconductor largely depends on the photon energy (or wavelength) of the light and various processes contribute to the dielectric function.

An overview of the electromagnetic spectrum in the optical range is given in Table 9.1. The energy and wavelength of a photon are related by<sup>1</sup>  $E = h\nu = hc/\lambda$ , i.e.

$$E \text{ [eV]} = \frac{1240}{\lambda \text{ [nm]}}. \quad (9.1)$$

In the infrared regime, energy is often measured in wave numbers ( $\text{cm}^{-1}$ ) for which the conversion  $1 \text{ meV} = 8.056 \text{ cm}^{-1}$  holds.

---

<sup>1</sup>The more exact numerical value in (9.1) is 1239.84.

**Table 9.1** Spectral ranges with relevance to semiconductor optical properties

Range		Wavelengths	Energies
Deep ultraviolet	DUV	<250 nm	>5 eV
Ultraviolet	UV	250–400 nm	3–5 eV
Visible	VIS	400–800 nm	1.6–3 eV
Near infrared	NIR	800 nm–2 μm	0.6–1.6 eV
Mid-infrared	MIR	2–20 μm	60 meV–0.6 eV
Far infrared	FIR	20–80 μm	1.6–60 meV
THz region	THz	>80 μm	<1.6 meV

## 9.2 Complex Dielectric Function

The dielectric function  $\epsilon$  fulfills

$$\mathbf{D} = \epsilon_0 \mathbf{E} + \mathbf{P} = \epsilon_0 \epsilon \mathbf{E}, \quad (9.2)$$

and is generally a rank 2 tensor since  $\mathbf{D}$  and  $\mathbf{E}$  must not be collinear. This is the case, e.g. for birefringence as discussed in Sect. 13.2.2. The general form of the dielectric tensor for various crystal symmetries is compiled in Table 9.2. In most cases in the following  $\epsilon$  will be used as scalar. The dielectric function is frequency dependent  $\epsilon(\omega)$  due to the various oscillators playing a role and decreases (non-monotonically) from its static value (for  $\omega = 0$ ) to 1 for  $\omega \rightarrow \infty$ . In some cases also its  $\mathbf{k}$ -dependence is important, known as spatial dispersion (cmp. Sect. 9.6.8). The dielectric function is generally complex and written as

$$\epsilon = \epsilon' + i \epsilon''. \quad (9.3)$$

The real and the imaginary part of the dielectric function are related to each other via the Kramers–Kronig relations (Appendix C).

The complex index of refraction is

$$n^* = n_r + i \kappa = \sqrt{\epsilon}. \quad (9.4)$$

From  $n^{*2}$  follows

$$\epsilon' = n_r^2 - \kappa^2 \quad (9.5)$$

$$\epsilon'' = 2 n_r \kappa. \quad (9.6)$$

From  $\epsilon \bar{\epsilon} = (n_r^2 + \kappa^2)^2$  and (9.5) follows

**Table 9.2** General form of the dielectric tensor for various crystals

crystal system optical symmetry		examples
cubic	isotropic	$\begin{pmatrix} a & 0 & 0 \\ 0 & a & 0 \\ 0 & 0 & a \end{pmatrix}$ Si, GaAs, MgO, ZnSe, CuI
tetragonal hexagonal trigonal	uniaxial	$\begin{pmatrix} a & 0 & 0 \\ 0 & a & 0 \\ 0 & 0 & c \end{pmatrix}$ CuGaSe <sub>2</sub> , GaN, Bi <sub>2</sub> Se <sub>3</sub>
orthorhombic	biaxial	$\begin{pmatrix} a & 0 & 0 \\ 0 & b & 0 \\ 0 & 0 & c \end{pmatrix}$ Sb <sub>2</sub> Se <sub>3</sub>
monoclinic	biaxial	$\begin{pmatrix} a & d & 0 \\ d & b & 0 \\ 0 & 0 & c \end{pmatrix}$ $\beta$ -Ga <sub>2</sub> O <sub>3</sub> , anthracene
triclinic	biaxial	$\begin{pmatrix} a & d & e \\ d & b & f \\ e & f & c \end{pmatrix}$ tetracene

$$n_r^2 = \frac{\epsilon' + \sqrt{\epsilon'^2 + \epsilon''^2}}{2} \tag{9.7}$$

$$\kappa = \frac{\epsilon''}{2n_r}. \tag{9.8}$$

The real part of the complex index of refraction  $n_r$  is responsible for the dispersion, the imaginary part  $\kappa$  is named extinction coefficient and is related to the absorption coefficient of the plane wave (damping of  $\mathbf{E}^2$ ) by

$$\alpha = 2 \frac{\omega}{c} \kappa = \frac{4\pi}{\lambda} \kappa = 2k \kappa. \tag{9.9}$$

Here,  $k$  and  $\lambda$  denote the respective values in vacuum.

### 9.3 Reflection and Diffraction

From Maxwell’s equations and the boundary conditions at a planar interface between two media with different index of refraction for the components of the electric and magnetic fields the laws for reflection and diffraction are derived. We denote the index of refraction as  $n$  and also  $n_r$  in the following. The interface between two media with refractive indices  $n_1$  and  $n_2$  is depicted in Fig. 9.1. In the following we assume first that no absorption occurs.

Snellius' law for the angle of diffraction is

$$n_1 \sin \phi = n_2 \sin \psi. \tag{9.10}$$

When the wave enters the denser medium, it is diffracted towards the normal. If the wave propagates into the less-dense medium (reversely to the situation shown in Fig. 9.1), a diffracted wave occurs only up to a critical angle of incidence

$$\sin \phi_{TR} = \frac{n_2}{n_1}. \tag{9.11}$$

For larger angles of incidence, total internal reflection occurs and the wave remains in the denser medium. Thus, the angle in (9.11) is called the critical angle for total reflection. For GaAs and air the critical angle is rather small,  $\phi_{TR} = 17.4^\circ$ .

The reflectance depends on the polarization (Fresnel formulas). The index 'p' ('s') denotes parallel polarized/TM (perpendicular polarized/TE) waves.

$$R_p = \left( \frac{\tan(\phi - \psi)}{\tan(\phi + \psi)} \right)^2 \tag{9.12}$$

$$R_s = \left( \frac{\sin(\phi - \psi)}{\sin(\phi + \psi)} \right)^2. \tag{9.13}$$

The situation for GaAs and air is shown for both polarization directions and unpolarized radiation in Fig. 9.2 for a wave going into and out of the GaAs.

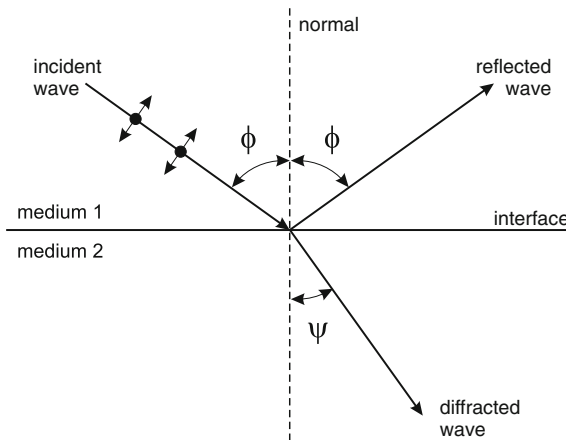


**Fig. 9.1** Reflection and diffraction of an electromagnetic wave at the transition between medium '1' and '2',  $n_2 > n_1$ . The polarization plane is defined by the surface normal and the  $k$ -vector of the light (plane of incidence). The parallel ('p') polarized wave (TM-wave, electric field vector oscillates in the plane) is shown as ' $\leftrightarrow$ '; perpendicular ('s') polarization (TE-wave, electric field vector is perpendicular to plane) is depicted as ' $\rightarrow$ '.

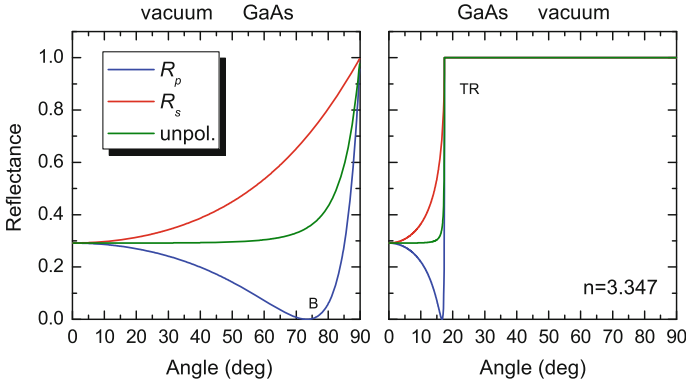


**Fig. 9.2** Reflectance of the GaAs/vacuum interface (close to the band gap,  $n_r = 3.347$ ) for radiation from vacuum/air (*left panel*) and from the GaAs (*right panel*), respectively, as a function of incidence angle and polarization

When the reflected and the diffracted wave are perpendicular to each other, the reflectance of the p-polarized wave is zero. This angle is the Brewster angle  $\phi_B$ ,

$$\tan \phi_B = \frac{n_2}{n_1}. \tag{9.14}$$

If a wave has vertical incidence from vacuum on a medium with index of refraction  $n_r$ , the reflectance is given (both polarizations are degenerate) as

$$R = \left( \frac{n_r - 1}{n_r + 1} \right)^2. \tag{9.15}$$

For GaAs, the reflectance for vertical incidence is 29.2%.

### 9.4 Absorption

In the absorption process, energy is transferred from the electromagnetic field to the semiconductor. In the case of a linear absorption process, when the probability of light absorption is proportional to the incoming intensity, the decrease of intensity in the absorbing medium is exponential (Lambert–Beer’s law [725, 726]),<sup>2</sup>

$$I(x) = I(0) \exp(-\alpha x). \tag{9.16}$$

<sup>2</sup>In [726], the absorption coefficient  $\mu$  was defined via  $I(d)/I(0) = \mu^d$ , i.e.  $\mu = \exp -\alpha$ .

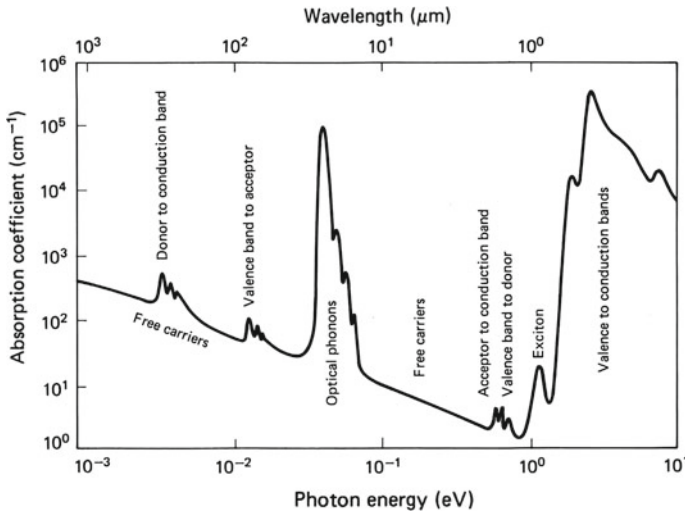


Fig. 9.3 Schematic absorption spectrum of a typical semiconductor. From [727]

The quantity  $\alpha$  is the *absorption coefficient*, its reverse the absorption depth. The spectral dependence  $\alpha(E)$ , the absorption spectrum, contains the information of the possible absorption processes, their energy, momentum and angular momentum selection rules, and their oscillator strength.

In Fig. 9.3 a schematic absorption spectrum of a semiconductor is depicted. The transition of electrons from the valence to the conduction band begins at the band gap energy. The band gaps of Si, Ge, GaAs, InP, InAs, InSb are in the IR, those of AlAs, GaP, AlP, InN in the VIS, those of GaN and ZnO in the UV, MgO and AlN are in the deep UV. The Coulomb correlation of electrons and holes leads to the formation of excitons that leads to absorption below the band gap. The typical excitation binding energy is in the range of 1–100 meV (see Fig. 9.16). Optical transitions from valence-band electrons into donors and from electrons on acceptors into the conduction band lead to band–impurity absorption. In the region from 10–100 meV the interaction with lattice vibrations (phonons) leads to absorption if the phonons are infrared active. Further in the FIR lie transitions from impurities to the closest band edge (donor to conduction and acceptor to valence band). A continuous background is due to free-carrier absorption.

If absorption is considered, the reflectance (9.15) needs to be modified. Using the complex index of refraction  $n^* = n_r + i\kappa$ , it is given as

$$R = \left| \frac{n^* - 1}{n^* + 1} \right|^2 = \frac{(n_r - 1)^2 + \kappa^2}{(n_r + 1)^2 + \kappa^2}. \quad (9.17)$$

## 9.5 Electron–Photon Interaction

The absorption process is quantum mechanically described by the coupling of electrons and photons. The process is described with time-dependent perturbation theory. If  $\mathbf{H}_{\text{em}}$  is the perturbation operator (electromagnetic field), the transition probability per time  $w_{\text{fi}}$  for electrons from (unperturbed) state ‘i’ (initial) to state ‘f’ (final) is given (with certain approximations) by Fermi’s golden rule

$$w_{\text{fi}}(\hbar\omega) = \frac{2\pi}{\hbar} |H'_{\text{fi}}|^2 \delta(E_f - E_i - \hbar\omega), \quad (9.18)$$

where  $\hbar\omega$  is the photon energy,  $E_i$  ( $E_f$ ) is the energy of the initial (final) state.  $H'_{\text{fi}}$  is the matrix element

$$H'_{\text{fi}} = \langle \Psi_f | \mathbf{H}' | \Psi_i \rangle, \quad (9.19)$$

where  $\Psi_i$  ( $\Psi_f$ ) are the wavefunctions of the unperturbed initial (final) state.

$\mathbf{A}$  is the vector potential for the electromagnetic field, i.e.  $\mathbf{E} = -\dot{\mathbf{A}}$ ,  $\mu\mathbf{H} = \nabla \times \mathbf{A}$ ,  $\nabla \cdot \mathbf{A} = 0$  (Coulomb gauge). The Hamiltonian of an electron in the electromagnetic field is

$$\mathbf{H} = \frac{1}{2m} (\hbar\mathbf{k} - q\mathbf{A})^2. \quad (9.20)$$

When terms in  $\mathbf{A}^2$  are neglected (i.e. two-photon processes), the perturbation Hamiltonian is thus

$$\mathbf{H}_{\text{em}} = -\frac{q}{m} \mathbf{A} \mathbf{p} = \frac{i\hbar q}{m} \mathbf{A} \cdot \nabla \approx q \mathbf{r} \cdot \mathbf{E}. \quad (9.21)$$

The latter approximation is valid for small wavevectors of the electromagnetic wave and is termed the *electric dipole approximation*.

In order to calculate the dielectric function of the semiconductor from its band structure we assume that  $\mathbf{A}$  is weak and we can apply (9.18). The transition probability  $R$  for the photon absorption rate at photon energy  $\hbar\omega$  is then given by<sup>3</sup>

$$R(\hbar\omega) = \frac{2\pi}{\hbar} \int_{\mathbf{k}_c} \int_{\mathbf{k}_v} | \langle c | \mathbf{H}_{\text{em}} | v \rangle |^2 \delta(E_c(\mathbf{k}_c) - E_v(\mathbf{k}_v) - \hbar\omega) d^3\mathbf{k}_c d^3\mathbf{k}_v, \quad (9.22)$$

with the Bloch functions  $|c\rangle$  and  $|v\rangle$  of the conduction and valence band, respectively, as given in (6.36b).

The vector potential is written as  $\mathbf{A} = A\hat{\mathbf{e}}$  with a unit vector  $\hat{\mathbf{e}}$  parallel to  $\mathbf{A}$ . The amplitude is connected to the electric-field amplitude  $E$  via

---

<sup>3</sup>Here we assume that the valence-band states are filled and the conduction-band states are empty. If the conduction-band states are filled and the valence-band states are empty, the rate is that of stimulated emission.

$$A = -\frac{E}{2\omega} [\exp(i(\mathbf{q}\mathbf{r} - \omega t)) + \exp(-i(\mathbf{q}\mathbf{r} - \omega t))]. \quad (9.23)$$

In the electric-dipole approximation the momentum conservation  $\mathbf{q} + \mathbf{k}_v = \mathbf{k}_c$ ,  $\mathbf{q}$  being the momentum of the light wave is approximated by  $\mathbf{k}_v = \mathbf{k}_c$ . The matrix element is then given by

$$|\langle c | \mathbf{H}_{em} | v \rangle|^2 = \frac{e^2 |A|^2}{m^2} |\langle c | \hat{\mathbf{e}} \cdot \mathbf{p} | v \rangle|^2, \quad (9.24)$$

with

$$\langle c | \hat{\mathbf{e}} \cdot \mathbf{p} | v \rangle|^2 = \frac{1}{3} |\mathbf{p}_{cv}|^2 = M_b^2, \quad (9.25)$$

and the momentum matrix element  $\mathbf{p}_{cv}$  given in (6.35). A  $\mathbf{k}$ -independent matrix element  $|\mathbf{p}_{cv}|^2$  is often used as an approximation. In Fig. 9.4 the matrix elements for valence to conduction band transitions in GaN are shown as a function of  $\mathbf{k}$ .

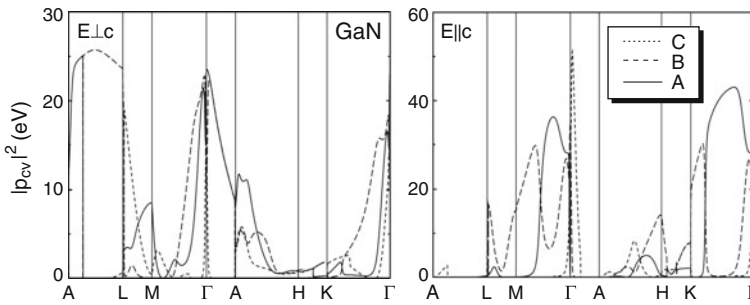


**Fig. 9.4** Theoretical momentum matrix elements  $|p_{cv}|^2$  along high-symmetry directions in the Brillouin zone (see Fig. 3.34d) for transitions between valence and conduction bands in GaN and light polarized perpendicular (*left panel*) and parallel (*right panel*) to the  $c$ -axis. The transitions are A:  $\Gamma_9(A) \rightarrow \Gamma_{7c}$ , B:  $\Gamma_7(B) \rightarrow \Gamma_{7c}$ , C:  $\Gamma_7(C) \rightarrow \Gamma_{7c}$  (see Fig. 6.38). Adapted from [728]

In terms of the electric-field amplitude  $E(\omega)$  the transition probability is

$$R(\hbar\omega) = \frac{2\pi}{\hbar} \left( \frac{e}{m\omega} \right)^2 \left| \frac{E(\omega)}{2} \right|^2 |\mathbf{p}_{cv}|^2 \int_{\mathbf{k}} \delta(E_c(\mathbf{k}) - E_v(\mathbf{k}) - \hbar\omega) d^3\mathbf{k}. \quad (9.26)$$

If the integration over  $\mathbf{k}$  is restricted to those values allowed in unit volume, the power that is lost from the field in unit volume is given by  $R \hbar \omega$ , leaving a  $1/E$  factor. The dielectric function  $\epsilon = \epsilon_r + i\epsilon_i$  is given by

$$\epsilon_i = \frac{1}{4\pi\epsilon_0} \left( \frac{2\pi e}{m\omega} \right)^2 |\mathbf{p}_{cv}|^2 \int_{\mathbf{k}} \delta(E_c(\mathbf{k}) - E_v(\mathbf{k}) - \hbar\omega) d^3\mathbf{k} \quad (9.27a)$$

$$\epsilon_r = 1 + \int_{\mathbf{k}} \frac{e^2}{\epsilon_0 m \omega_{cv}^2} \frac{2 |\mathbf{p}_{cv}|^2}{m \hbar \omega_{cv}} \frac{1}{1 - \omega^2/\omega_{cv}^2} d^3\mathbf{k}, \quad (9.27b)$$

with  $\hbar\omega_{cv} = E_c(\mathbf{k}) - E_v(\mathbf{k})$ . The second equation has been obtained via the Kramers–Kronig relations<sup>4</sup> (see Appendix C).

Comparison with (D.7) yields that the oscillator strength of the band–band absorption is given by

$$f = \frac{e^2}{\epsilon_0 m \omega_{cv}^2} \frac{2 |\mathbf{p}_{cv}|^2}{m \hbar \omega_{cv}}, \quad (9.28)$$

with

$$N_{cv} = \frac{2 |\mathbf{p}_{cv}|^2}{m \hbar \omega_{cv}} \quad (9.29)$$

being the classical ‘number’ of oscillators with the frequency  $\omega_{cv}$ .

## 9.6 Band–Band Transitions

### 9.6.1 Joint Density of States

The strength of an allowed optical transitions between valence and conduction bands is proportional to the joint density of states (JDOS)  $D_j(E_{cv})$  (cf. (6.59), (6.60) and (9.27a))

$$D_j(E_{cv}) = 2 \int_{S(\tilde{E})} \frac{d^2S}{(2\pi/L)^3} \frac{1}{|\nabla_{\mathbf{k}} E_{cv}|}, \quad (9.30)$$

where  $E_{cv}$  is an abbreviation for  $E_c(\mathbf{k}) - E_v(\mathbf{k})$  and  $d^2S$  is a surface element of the constant energy surface with  $\tilde{E} = E_{cv}$ . The spin is assumed to generate doubly degenerate bands and accounts for the pre-factor 2. Singularities of the JDOS (*van-Hove singularities* or *critical points*) appear where  $\nabla_{\mathbf{k}} E_{cv}$  vanishes. This occurs when the gradient for both bands is zero or when both bands are parallel. The latter generates particularly large JDOS because the condition is valid at many points in  $\mathbf{k}$ -space.

<sup>4</sup>The real and imaginary parts of the dielectric function are generally related to each other via the Kramers–Kronig relations.

**Table 9.3** Functional dependence of the joint density of states for critical points in 3, 2 and 1 dimensions

Dim.	Label	Type	$D_j$ for $E < E_0$	$D_j$ for $E > E_0$
3D	$M_0$	Min.	0	$\sqrt{E - E_0}$
	$M_1$	Saddle	$C - \sqrt{E_0 - E}$	$C$
	$M_2$	Saddle	$C$	$C - \sqrt{E - E_0}$
	$M_3$	Max.	$\sqrt{E_0 - E}$	0
2D	$M_0$	Min.	0	$C$
	$M_1$	Saddle	$-\ln(E_0 - E)$	$-\ln(E - E_0)$
	$M_2$	Max.	$C$	0
1D	$M_0$	Min.	0	$\sqrt{E - E_0}$
	$M_1$	Max.	$\sqrt{E_0 - E}$	0

$E_0$  denotes the energy (band separation) at the critical point,  $C$  stands for a constant value. The type of critical point is given (min.: minimum, saddle: saddle point, max.: maximum)

Generally, the (three-dimensional) energy dispersion  $E(\mathbf{k})$  around a three-dimensional critical point (here developed at  $\mathbf{k} = 0$ ) can be written as

$$E(\mathbf{k}) = E(0) + \frac{\hbar^2 k_x^2}{2m_x} + \frac{\hbar^2 k_y^2}{2m_y} + \frac{\hbar^2 k_z^2}{2m_z}. \quad (9.31)$$

The singularities are classified as  $M_0$ ,  $M_1$ ,  $M_2$  and  $M_3$  with the index being the number of masses  $m_i$  in (9.31) that are negative.  $M_0$  ( $M_3$ ) describes a minimum (maximum) of the band separation.  $M_1$  and  $M_2$  are saddle points. For a two-dimensional  $\mathbf{k}$ -space there exist  $M_0$ ,  $M_1$  and  $M_2$  points (minimum, saddle point and maximum, respectively). For a one-dimensional  $\mathbf{k}$ -space there exist  $M_0$  and  $M_1$  points (minimum and maximum, respectively). The functional dependence of the JDOS at the critical points is summarized in Table 9.3. The resulting shape of the dielectric function is visualized in Fig. 9.5.

## 9.6.2 Direct Transitions

Transitions between states at the band edges at the  $\Gamma$  point are possible (Fig. 9.6). The  $\mathbf{k}$  conservation requires (almost) vertical transitions in the  $E(\mathbf{k})$  diagram because the length of the light  $\mathbf{k}$  vector,  $k = 2\pi/\lambda$ , is much smaller than the size of the Brillouin zone  $|k| \leq \pi/a_0$ . The ratio of the lengths of the  $\mathbf{k}$  vectors is of the order  $a_0/\lambda$  and typically about  $10^{-3}$  for NIR wavelengths.

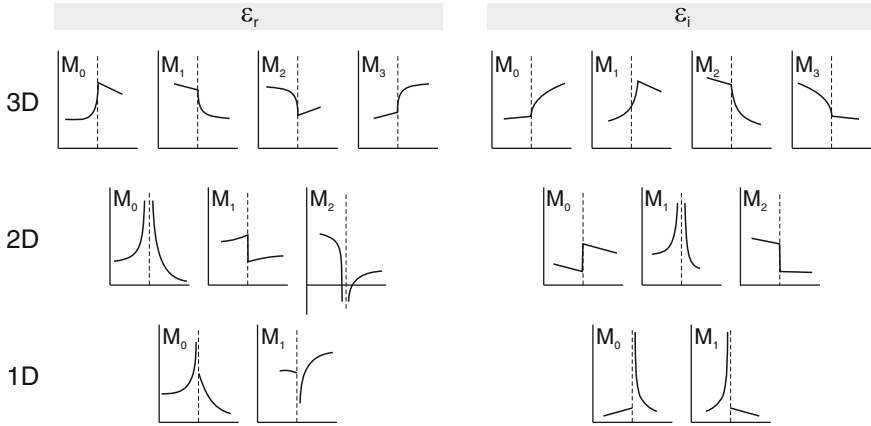


**Fig. 9.5** Shape of the real (*left panel*) and imaginary (*right panel*) parts of the dielectric function in the vicinity of critical points in 3, 2 and 1 dimensions (for labels see Table 9.3). The *dashed line* in each graph indicates the energy position of the critical point  $E_0$ . Adapted from [729]

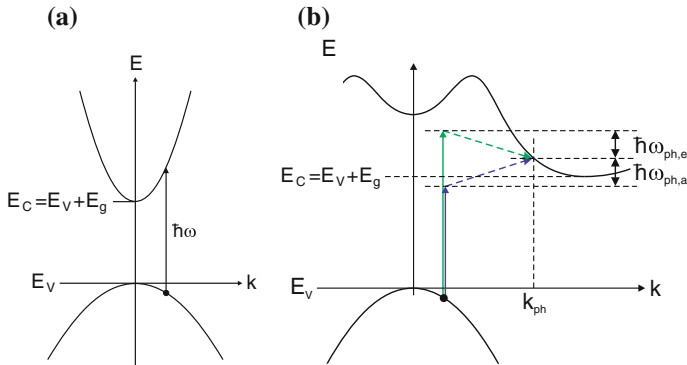


**Fig. 9.6** (a) Direct optical transition and (b) indirect optical transitions between valence and conduction bands. The indirect transition involves a phonon with energy  $\hbar\omega_{ph}$  (index *a*: phonon absorption, *e*: phonon emission) and wavevector  $k_{ph}$

For isotropic parabolic bands the band-band transition energy versus wavevector relation is

$$E_{cv}(k) = E_g + \frac{\hbar^2}{2} \left( \frac{1}{m_e^*} + \frac{1}{m_h^*} \right) k^2. \tag{9.32}$$

When the energy dependence of the matrix element is neglected, the absorption coefficient is determined by the corresponding square-root joint density of states ( $M_0$  critical point):

$$\alpha(E) \propto \frac{\sqrt{E - E_g}}{E} \approx \alpha \sqrt{E - E_g}. \tag{9.33}$$

The approximation is valid if the considered energy interval, e.g. around a band edge, is small.

Absorption spectra of  $(\text{In}_x\text{Ga}_{1-x})_2\text{O}_3$  alloy thin films at room temperature are shown in Fig. 9.7a. The  $\alpha^2$  versus photon energy plots shows a linear dependence with broadening and additional states at the band edge due to disorder effects. The extrapolation of the linear parts yields the absorption edge (Fig. 9.7b).

Absorption spectra of GaAs are shown in Fig. 9.8a for photon energies close to the band gap at various temperatures. The rapid increase, typical for direct semiconductors, is obvious. In particular at low temperatures, however, the absorption lineshape close to the band gap is dominated by an excitonic feature, discussed in Sect. 9.6.6.

Due to the increasing density of states, the absorption increases with the photon energy (Fig. 9.8c). At 1.85 eV there is a step in the absorption spectrum of GaAs due to the beginning of the contribution of transitions between the s-o hole band and the conduction band (see  $E_0 + \Delta_0$  transition in Fig. 9.8e). When bands run in parallel, i.e. with the same separation, in the  $E(\mathbf{k})$  diagram, the absorption processes accumulate at the same transition energy. In this way higher peaks in the absorption spectrum due to the  $E_1$  or  $E'_0$  transitions originate as indicated in the band structure in Fig. 9.8e.

The selection rules for transitions from valence to conduction band must take into account the angular momentum and spin states of the wavefunctions. The optical transitions for circularly polarized light are shown in Fig. 9.9a, fulfilling the selection rule  $\Delta m_j = \pm 1$ . A lifting of the energetic degeneracies of these states occurs, e.g. by magnetic fields or spatial confinement (cmp. Fig. 12.29). For two-photon absorption (Sect. 9.6.14), the selection rule is  $\Delta m_j = \pm 2$  as shown in Fig. 9.9b [732].

We note that in some materials the direct transition between certain bands is forbidden. An example is  $\text{SnO}_2$  where the direct transition from the topmost valence

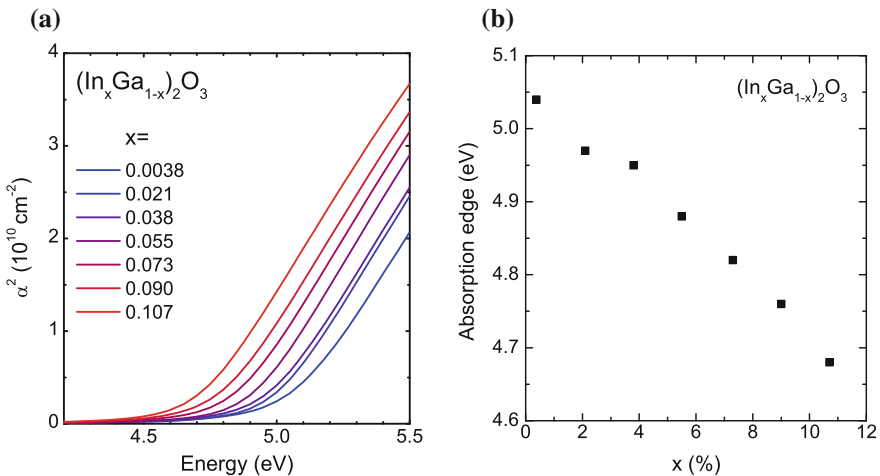


**Fig. 9.7** (a) Absorption spectra of  $(\text{In}_x\text{Ga}_{1-x})_2\text{O}_3$  alloy thin films on  $\text{Al}_2\text{O}_3$ , plotted as  $\alpha^2$  versus photon energy. (b) Band edge determined from extrapolation of linear parts

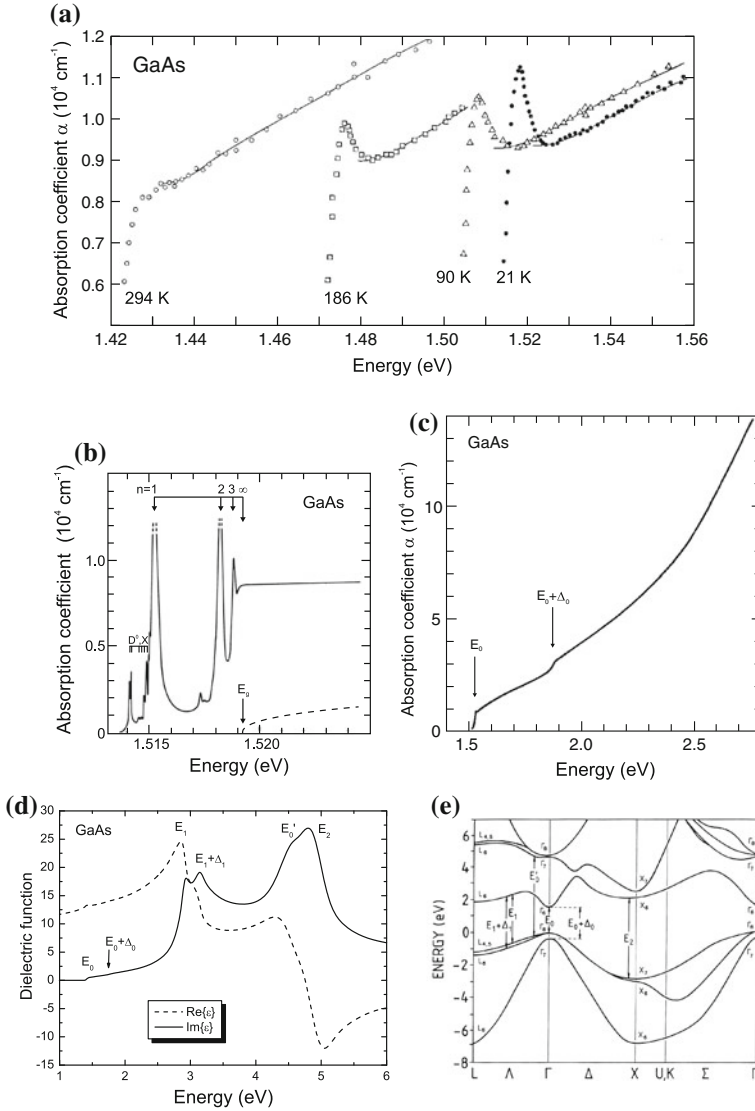


**Fig. 9.8** (a) Absorption of GaAs close to the band gap at different temperatures. Adapted from [730]. (b) High-resolution absorption spectrum of highly pure GaAs at  $T = 1.2 \text{ K}$  in the exciton region. *Dashed line* is theory without excitonic correlation. Adapted from [731]. (c) Absorption spectrum of GaAs at  $T = 21 \text{ K}$  in the vicinity of the band gap. Adapted from [730]. (d) Complex dielectric function of GaAs at  $T = 300 \text{ K}$ , *dashed (solid) line* real (imaginary) part of dielectric constant. Peak labels relate to transitions shown in part (e). (e) Band structure of GaAs with band gap transition ( $E_0$ ) and higher transitions ( $E_0 + \Delta_0$ ,  $E_1$ ,  $E_1 + \Delta_1$ ,  $E_0'$ , and  $E_2$ ) indicated

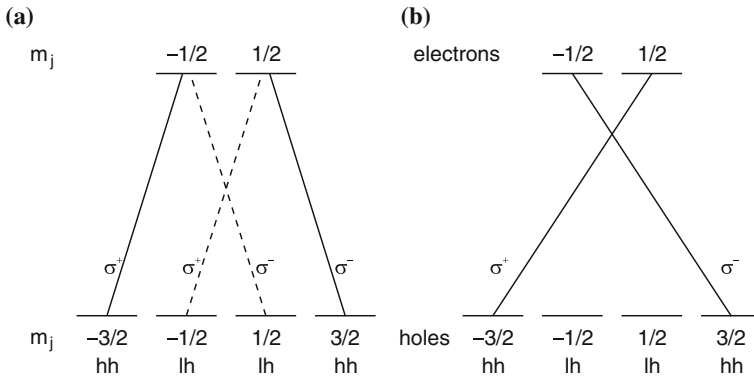


**Fig. 9.9** Optical selection rules for band–band transitions in bulk material for (a) single photon transitions and (b) two-photon transitions (with photon energy equal to half the transition energy)

band into the lowest conduction band (at  $\Gamma$ ) is forbidden (cmp. Fig.9.46). If the matrix element increases linearly with  $E - E_g$ , the absorption coefficient varies like

$$\alpha(E) \propto (E - E_g)^{3/2}. \tag{9.34}$$

### 9.6.3 Indirect Transitions

In an indirect band structure the missing  $\mathbf{k}$  difference (across the Brillouin zone) between valence- and conduction-band state needs to be provided by a second quantum. A phonon can provide the necessary momentum and additionally contributes a small amount of energy  $\hbar\omega_{\text{ph}}$ . There are several steps in the absorption spectrum due to various involved phonons (or combinations of them). At low temperature ( $T = 1.6\text{K}$ , Fig.9.10) phonons can only be generated and the absorption starts at energies *above* the band gap. At higher temperatures (typically above 40 K [733], Fig.9.10), acoustical phonons assisting the optical absorption transition can also be absorbed from the crystal; in this case due to energy conservation the absorption starts already at an energy  $E_g - \hbar\omega_{\text{ph}}$  *below* the band gap. At even higher temperatures ( $>200\text{K}$ , Fig.9.10), also optical phonons can be absorbed.

The perturbation calculation yields an absorption coefficient with a quadratic dependence on energy (9.35a) [734]. Essentially, for the absorption into a specific (empty) conduction band state (with square-root density of states) various initial (filled) valence band states (also with square-root density of states) are possible, making the probability depend on the product of the DOS and thus on the energy to the first power. Integrating over all energy states with energy separation  $E \pm \hbar\omega_{\text{ph}}$ , yields an  $E^2$ -dependence.<sup>5</sup> Considering the temperature dependent population of

<sup>5</sup>A flat optical phonon dispersion is assumed.

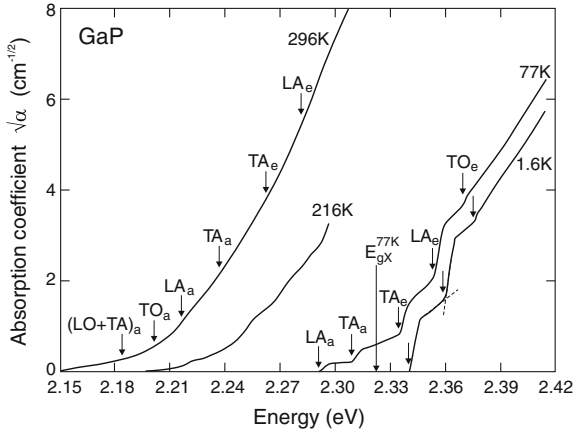


**Fig. 9.10** Absorption edge of GaP ( $\sqrt{\alpha}$  vs.  $E$ ) at various temperatures. The index ‘e’ (‘a’) indicates phonon emission (absorption) during the optical absorption process. The theoretical excitonic gap ( $E_{gX}$ ) at  $T = 77$  K is indicated. Adapted from [733]

the phonon density of states (Bose statistics, (E.3)) the absorption coefficients for transitions with phonon emission ( $\alpha_e$ ) and phonon absorption ( $\alpha_a$ ) are:

$$\alpha_e(E) \propto \frac{(E - (E_g + \hbar\omega_{ph}))^2}{1 - \exp(-\hbar\omega_{ph}/kT)} \tag{9.35a}$$

$$\alpha_a(E) \propto \frac{(E - (E_g - \hbar\omega_{ph}))^2}{\exp(\hbar\omega_{ph}/kT) - 1} \tag{9.35b}$$

The two-particle process is less probable than the direct absorption that only involves one photon. The strength of indirect absorption close to the band gap is about  $10^{-3}$  smaller than for the direct transition.

An 11-parameter formula based on terms like (9.35a) can describe the room temperature absorption spectrum of silicon in the visible with a precision of a few percent [735].

The absorption spectra close to the absorption edge are shown for GaP (Fig. 9.10) and Si (Fig. 9.11a). According to (9.35a), the plot of  $\sqrt{\alpha}$  versus energy (Macfarlane–Roberts plot [736]) yields a straight line beyond the spectral region of phonon effects. The complicated form close to the (indirect) gap energy is due to the contribution of different phonons. The phonon energies found to contribute to the silicon absorption edge [737] agree with the TA and TO energy at the X minimum [738] (Fig. 9.11b). Also multiple phonons can contribute (Fig. 9.10). The momentum conservation can also be achieved by impurity scattering or electron–electron scattering [739].

We note also that the indirect semiconductors have an optical transition between  $\Gamma$  valence- and conduction-band states. However, this transition is at higher energies than the fundamental band gap, e.g. for Si ( $E_g = 1.12$  eV) at 3.4 eV (see Fig. 6.6a). In

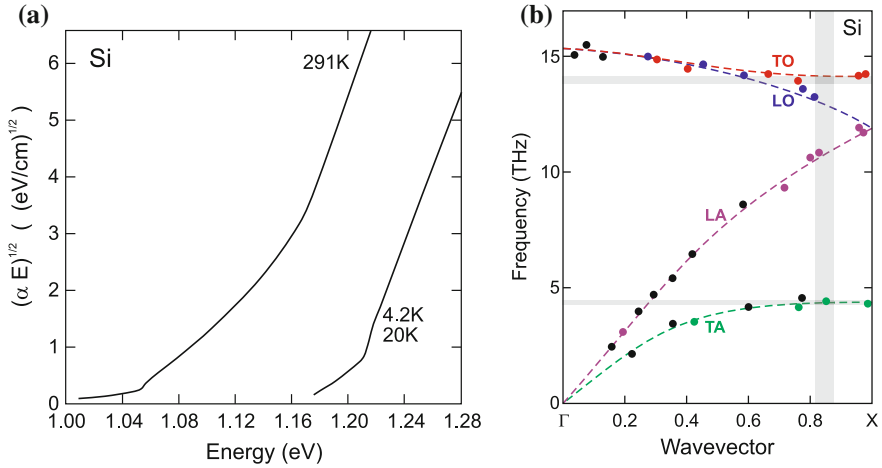


**Fig. 9.11** (a) Absorption edge of Si at two different temperatures. Adapted from [737]. (b) Phonon energies in silicon along [001] obtained from neutron scattering (black unidentified, green TA, purple LA, blue LO, red TO). The vertical grey bar indicates the position of the conduction band minimum, the horizontal grey bars the energies of the phonons observed at the indirect optical absorption edge. The dark grey overlap areas indicate that TO and TA phonons contribute. Adapted from [738]

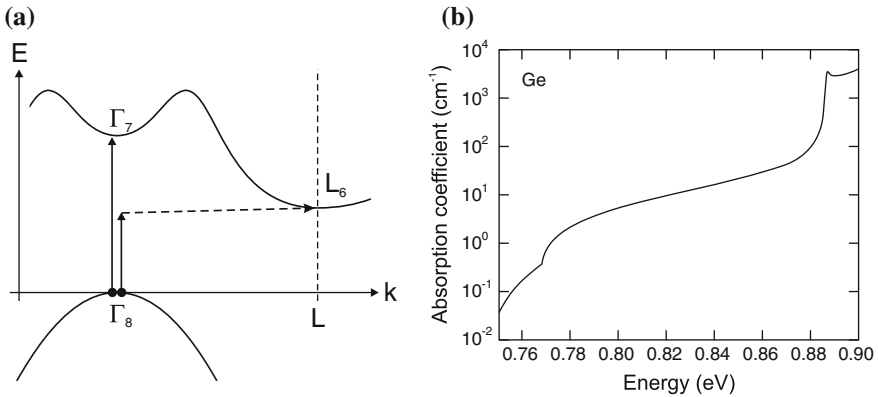


**Fig. 9.12** (a) Scheme of indirect and direct optical transitions starting at the top of the valence band in Ge. Vertical solid lines represent the involved photon, the horizontal dashed line the involved phonon. (b) Experimental absorption spectrum of Ge ( $T = 20$  K). Adapted from [737]

Fig. 9.12, the absorption scheme for indirect and direct absorption processes starting with an electron at the top of the valence band is shown together with an experimental absorption spectrum for Ge with the direct transition ( $\Gamma_8 \rightarrow \Gamma_7$ ) at 0.89 eV, 0.136 eV above the fundamental band gap.

In Fig. 9.13, the absorption edge of BaTiO<sub>3</sub> is shown. An indirect transition with an increase of (weak) absorption  $\propto E^2$  and an indirect gap of  $E_i = 2.66$  eV and a

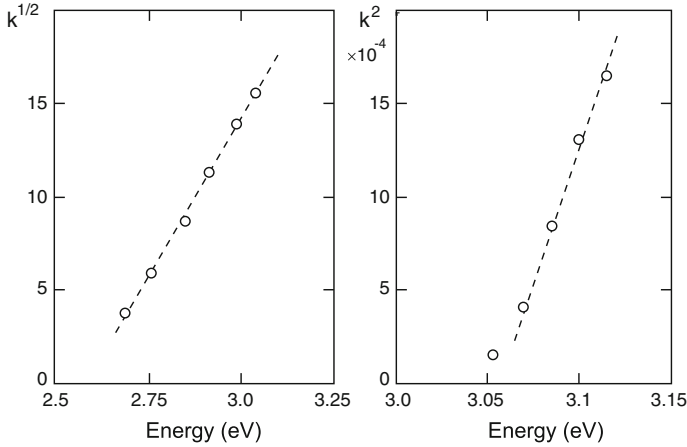


**Fig. 9.13** Absorption of BaTiO<sub>3</sub> at room temperature. Experimental data (*circles*) from [740] with fits (*dashed lines*)  $\propto E^2$  and  $\propto E^{1/2}$ , respectively

direct transition with an increase of (strong) absorption  $\propto E^{1/2}$  and a direct gap of  $E_d = 3.05$  eV are observed. These transitions could be due to holes at the M (indirect gap) and  $\Gamma$  (direct gap) points (cf. Sect. 6.3.11), respectively.

### 9.6.4 Urbach Tail

Instead of the ideal  $(E - E_g)^{1/2}$  dependence of the direct band-edge absorption, often an exponential tail is observed (see Fig. 9.14). This tail is called the Urbach tail [741] and follows the functional dependence (for  $E < E_g$ )

$$\alpha(E) \propto \exp\left(\frac{E - E_g}{E_0}\right), \tag{9.36}$$

where  $E_0$  is the characteristic width of the absorption edge, the so-called Urbach parameter.

The Urbach tail is attributed to transitions between band tails below the band edges. Such tails can originate from disorder of the perfect crystal, e.g. from defects or doping, and the fluctuation of electronic energy bands due to lattice vibrations. The temperature dependence of the Urbach parameter  $E_0$  is thus related to that of the band gap as discussed in [742, 743].

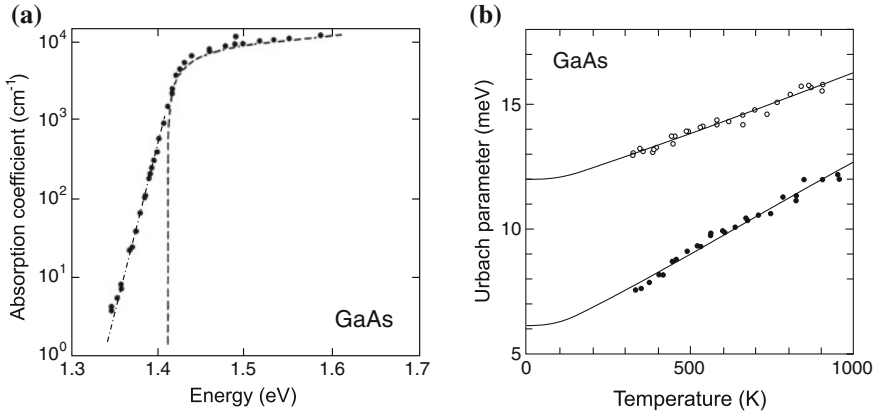
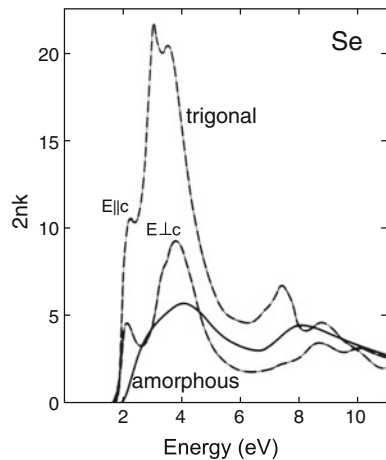


**Fig. 9.14** (a) Experimental absorption spectrum (*circles*) of GaAs at room temperature on a semi-logarithmic plot. The exponential tail below the band gap is called the Urbach tail (the *dash-dotted* line corresponds to  $E_0 = 10.3$  meV in (9.36)). The *dashed* line is the theoretical dependence from (9.33). Adapted from [744]. (b) Temperature dependence of Urbach parameter  $E_0$  for two GaAs samples. Experimental data for undoped (*solid circles*) and Si-doped ( $n = 2 \times 10^{18}$  cm $^{-3}$ , *empty circles*) GaAs and theoretical fits (*solid lines*) with one-phonon model. Adapted from [742]

### 9.6.5 Amorphous Semiconductors

The sharp features in the dielectric function due to critical points in the band structure of crystalline semiconductors are washed out in amorphous material. As an example the spectra of the imaginary part of the dielectric function for crystalline (trigonal) and amorphous selenium are shown in Fig. 9.15.

**Fig. 9.15** Imaginary part of the dielectric function of amorphous (*solid line*) and crystalline (trigonal) selenium (*dash-dotted lines* for two different polarization directions). From [745]



### 9.6.6 Excitons

An electron in the conduction band and a hole in the valence band form a hydrogen-like state due to the mutual Coulomb interaction. Such a state is called an exciton. The center-of-mass motion is separated and has a dispersion  $E = \frac{\hbar^2}{2M} \mathbf{K}^2$ , where  $M = m_e + m_h$  is the total mass and  $\hbar \mathbf{K}$  is the center-of-mass momentum

$$\mathbf{K} = \mathbf{k}_e + \mathbf{k}_h. \tag{9.37}$$

The relative motion yields hydrogen-like quantized states  $E_n \propto n^{-2}$  ( $n \geq 1$ ):

$$E_X^n = -\frac{m_r^*}{m_0} \frac{1}{\epsilon_r^2} \frac{m_0 e^4}{2(4\pi\epsilon_0 \hbar)^2} \frac{1}{n^2}, \tag{9.38}$$

where  $m_r^*$  denotes the reduced effective mass  $m_r^{*-1} = m_e^{*-1} + m_h^{*-1}$ . The third factor is the atomic Rydberg energy (13.6 eV). The exciton binding energy  $E_X^b = -E_X^1$  is scaled by  $(m^*/m_0) \epsilon_r^{-2} \approx 10^{-3}$ . A more detailed theory of excitons beyond the simple hydrogen model presented here, taking into account the valence-band structure, can be found in [746] for direct and [747] for indirect cubic and in [748] for wurtzite semiconductors. The exciton binding energies for various semiconductors are listed in Table 9.4 and shown in Fig. 9.16a versus the band gap.

The radius of the exciton is

$$r_X^n = n^2 \frac{m_0}{m_r^*} \epsilon_r a_B, \tag{9.39}$$

where  $a_B = 0.053$  nm denotes the hydrogen Bohr radius.<sup>6</sup> The Bohr radius of the exciton is  $a_X = r_X^1$  (14.6 nm for GaAs,  $\sim 2$  nm for ZnO). The exciton moves with the center-of-mass  $\mathbf{K}$ -vector through the crystal. The complete dispersion is (see Fig. 9.16b)

**Table 9.4** Exciton ( $E_X^b$ ) and biexciton ( $E_{XX}^b$ , see Sect. 9.6.10) binding energies in various bulk semiconductors

Material	$E_X^b$ (meV)	$E_{XX}^b$ (meV)	$E_{XX}^b/E_X^b$
GaAs	4.2		
GaAs QW	9.2	2.0	0.22
ZnSe	17	3.5	0.21
GaN	25	5.6	0.22
CdS	27	5.4	0.20
ZnS	37	8.0	0.22
ZnO	59	15	0.25

Values for 10 nm GaAs/15 nm  $Al_{0.3}Ga_{0.7}As$  quantum well (QW) are taken from [749]

<sup>6</sup>Cf. (7.20); an electron bound to a donor can be considered as an exciton with an infinite hole mass.

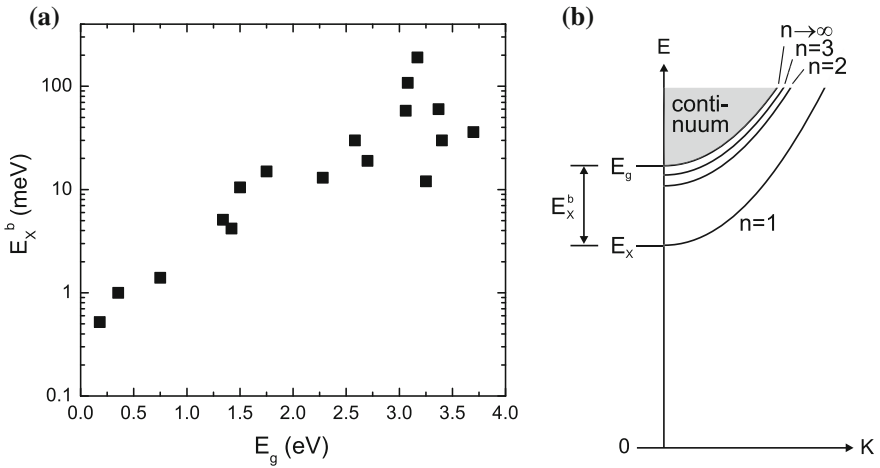


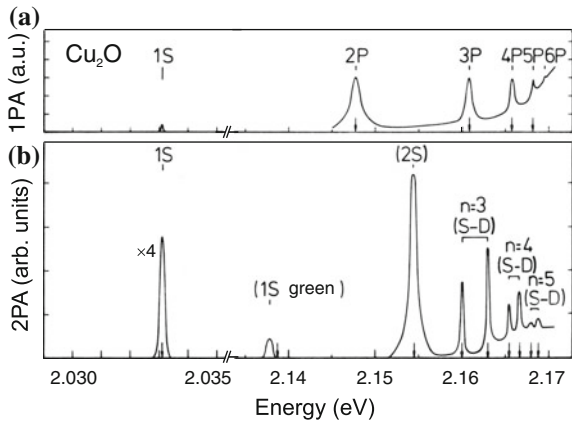
**Fig. 9.16** (a) Exciton binding energy versus band gap for various semiconductors. (b) Schematic dispersion of excitonic levels. The  $K$ -vector refers to the center-of-mass motion

$$E = E_g + E_X^n + \frac{\hbar^2}{2M} \mathbf{K}^2. \tag{9.40}$$

The oscillator strength of the exciton states decays  $\propto n^{-3}$ . The absorption due to excitons is visible in Fig. 9.8a for GaAs at low temperatures. If inhomogeneities are present, typically only the  $n = 1$  transition is seen. However, under special conditions also higher transitions of the exciton Rydberg series are seen (e.g.  $n = 2$  and 3 in Fig. 9.8b).

The exciton concept was introduced first for absorption in  $\text{Cu}_2\text{O}$  [750]. The  $J = 1/2$  absorption spectrum (‘yellow series’) is shown in Fig. 9.17. In this particular

**Fig. 9.17** One-photon (*top*) and two-photon (*bottom*) absorption spectra of  $\text{Cu}_2\text{O}$  at  $T = 4.2\text{K}$ . Arrows denote theoretical peak positions. Adapted from [752]



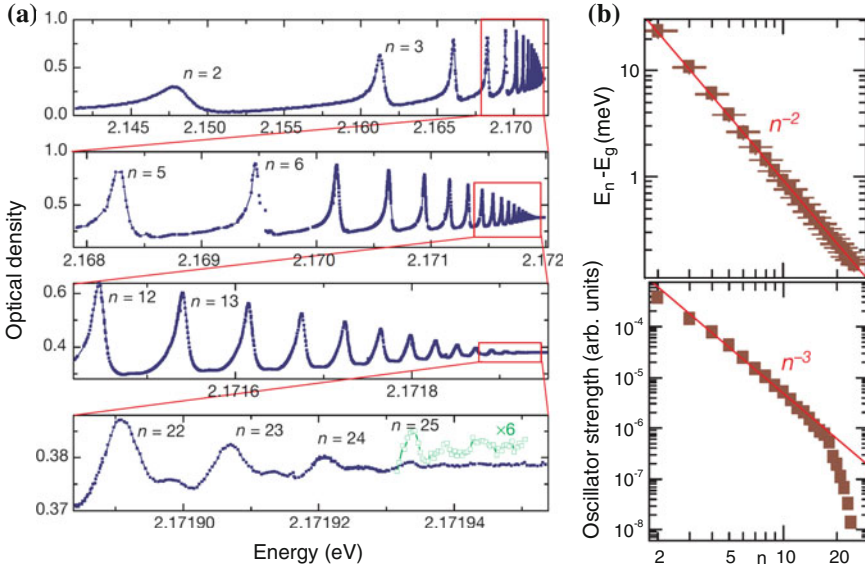


**Fig. 9.18** (One photon) Absorption spectrum of Cu<sub>2</sub>O (thickness 34 μm) at T = 1.2K with transitions labelled n = 2 . . . 25. Adapted from [751]

material both the valence and conduction bands have s character, thus the 1s transition of the exciton is forbidden and the np transitions are observed in normal (one-photon) absorption. With two-photon absorption also the s (and d) transitions can be excited. On a piece of natural Cu<sub>2</sub>O, the Rydberg series has been measured up to n = 25 [751] (Fig. 9.18a). The peak energy and the oscillator strength follow the n<sup>-2</sup> (E<sub>X</sub><sup>b</sup> = 92 meV, E<sub>g</sub> = 2.17208 eV) and n<sup>-3</sup> laws, respectively, expected from a hydrogen model (Fig. 9.18b). The deviation from the n<sup>-3</sup>-dependence for the oscillator strength at large n is due to interaction effects of excitons with large radius at finite exciton density.

The scattering (unbound) states of the exciton [753] for E > E<sub>g</sub> contribute to absorption above the band gap. The factor by which the absorption spectrum is changed is called the Sommerfeld factor. For bulk material it is

$$S(\eta) = \eta \frac{\exp(\eta)}{\sinh(\eta)}, \tag{9.41}$$

with  $\eta = \pi [E_X^b / (E - E_g)]^{1/2}$ . The change of the absorption spectrum due to the Coulomb correlation is shown in Fig. 9.19. There is a continuous absorption between the bound and unbound states. At the band gap there is a finite absorption ( $S(E \rightarrow E_g) \rightarrow \infty$ ). The detail to which exciton peaks can be resolved depends on the spectral broadening.

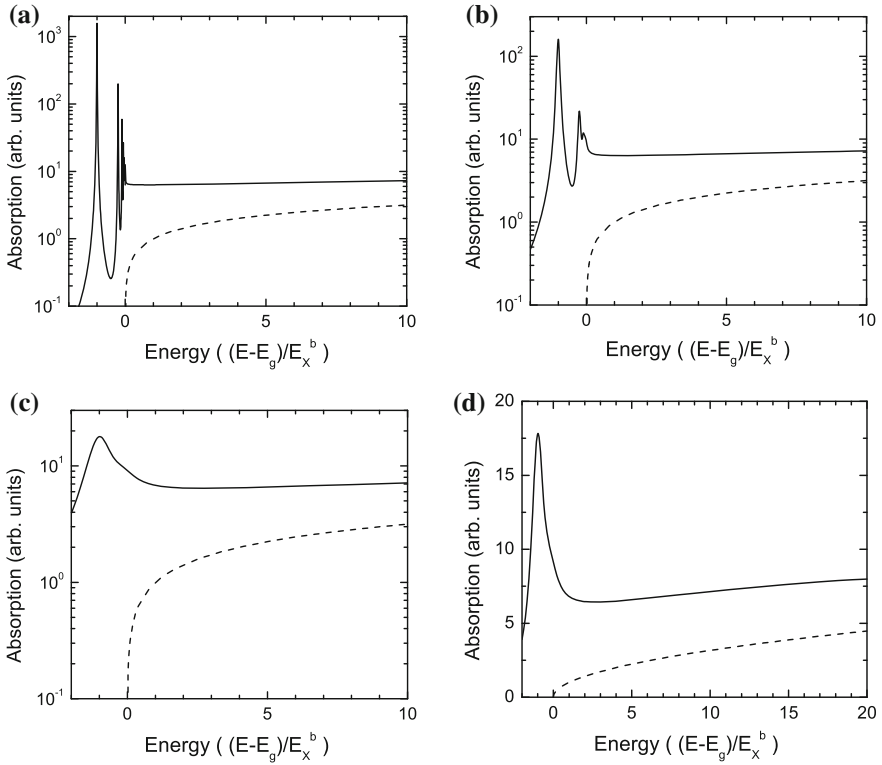


**Fig. 9.19** Modification of the absorption edge of a direct transition by excitonic effects for different spectral (Lorentzian) broadening ( $\propto (E^2 + \Gamma^2/4)^{-1}$ ), (a)  $\Gamma = 0.01 E_X^b$ , (b)  $\Gamma = 0.1 E_X^b$ , (c)  $\Gamma = E_X^b$ . (d) is (c) in linear scale. Dashed lines are electron–hole plasma absorption according to (9.33)

**Fig. 9.20** Theoretical dependency (lines) for the differences of the C-line and A-line as well as B-line and A-line exciton transition energies in GaN as a function of the *c*-axis strain. Symbols are experimental data from [754]. Adapted from [468]

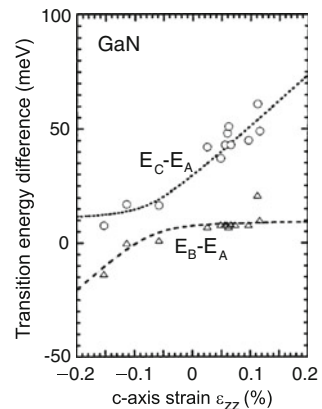


**Table 9.5** Phonon broadening parameters (FWHM) of various bulk semiconductors

Material	$\hbar\omega_{\text{LO}}$ (meV)	$\Gamma_0$ (meV)	$\gamma_{\text{AC}}$ ( $\mu\text{eV/K}$ )	$\gamma_{\text{LO}}$ (meV)
GaAs	36.8	0	$4 \pm 2$	$16.8 \pm 2$
ZnSe	30.5	1.9	$0 \pm 7$	$84 \pm 8$
GaN	92	10	$15 \pm 4$	$408 \pm 30$
ZnO	33	1.2	$32 \pm 26$	$96 \pm 24$

Values from fits with (9.42) to experimental data for GaAs [759], ZnSe [757], GaN [756], ZnO [760] (phonon energy fitted) as shown in Fig. 9.22b

In Fig. 9.20 the energy separations of the A-, B-, and C-excitons in GaN are shown [468]. Thus, the ordering of the valence bands depends on the strain state of the semiconductor.

### 9.6.7 Phonon Broadening

The scattering with phonons and the related dephasing leads to homogeneous broadening  $\Gamma_{\text{hom}}$  of absorption (and recombination) lines. Acoustic and optical phonons contribute to the broadening according to the dependence [755]

$$\Gamma_{\text{hom}}(T) = \Gamma_0 + \gamma_{\text{AC}} T + \gamma_{\text{LO}} \frac{1}{\exp(\hbar\omega_{\text{LO}}/kT) - 1}, \quad (9.42)$$

where  $\hbar\omega_{\text{LO}}$  is the optical phonon energy and the last factor is the Bose function (E.24).  $\Gamma_0$  is a temperature-independent contribution,  $\Gamma_0 = \Gamma(T = 0)$ . The increasing broadening with increasing temperature is obvious, e.g., in absorption spectra (Fig. 9.21a). In Fig. 9.21b experimental data for GaAs, ZnSe and GaN are assembled. The data have been fitted with (9.42); the resulting phonon broadening parameters are listed in Table 9.5.<sup>7</sup> The optical transitions in polar semiconductors exhibit stronger coupling to optical phonons. The phonon coupling parameters from different measurements on GaN are discussed and compared in [758].

### 9.6.8 Exciton Polariton

Electrons and holes are particles with spin 1/2. Thus, the exciton can form states with total spin  $S = 0$  (para-exciton, singlet) and  $S = 1$  (ortho-exciton, triplet). The

<sup>7</sup>Such parameter can be directly determined from spectroscopic broadening (as in [756]) or a time-resolved measurement of the decay of the coherent polarization (four-wave mixing) as in [757]. In the latter, the decay constant of the dephasing  $T_2$  is related to the decay constant  $\tau$  of the FWM-signal by  $T_2 = 2\tau$  for homogeneous broadening. The Fourier transform of  $\exp -t/(2\tau)$  is a Lorentzian of the type  $\propto ((E - E_0)^2 + \Gamma^2/4)^{-1}$  with  $\Gamma = 1/\tau$  being the FWHM.

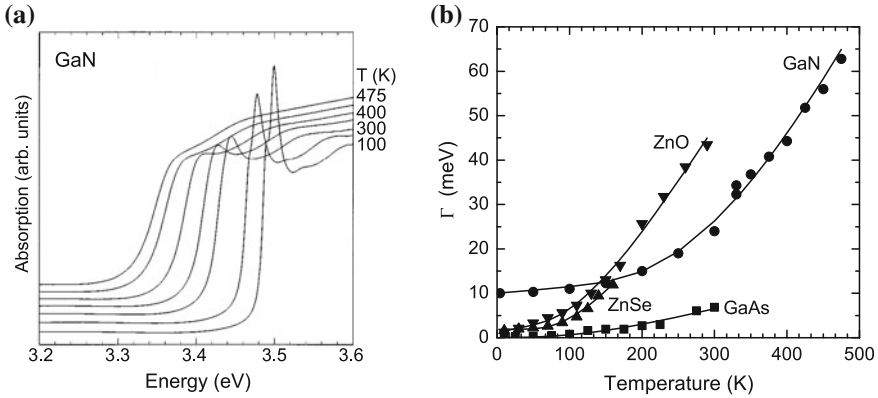


**Fig. 9.21** (a) Absorption spectra of GaN bulk ( $0.38\ \mu\text{m}$  thick epilayer on sapphire) for various temperatures  $T = 100, 200, 300, 350, 400, 450,$  and  $475\ \text{K}$ . Adapted from [756]. (b) Homogeneous broadening as a function of temperature, *symbols* are experimental data, *solid lines* are fits, cf. Table 9.5

exchange interaction leads to a splitting of these states, the singlet being the energetically higher. The singlet state splits into the longitudinal and transverse exciton with respect to the orientation of the polarization carried by the Bloch functions and the center-of-mass motion  $\mathbf{K}$  of the exciton. Dipole transitions are only possible for singlet excitons (bright excitons). The triplet excitons couple only weakly to the electromagnetic field and are thus also called dark excitons.

The coupling of these states to the electromagnetic field creates new quasi-particles, the exciton polaritons [761, 762]. The dielectric function of the exciton (with background dielectric constant  $\epsilon_b$ ) is

$$\epsilon(\omega) = \epsilon_b \left[ 1 + \frac{\beta}{1 - (\omega^2/\omega_X)^2} \right] \cong \epsilon_b \left[ 1 + \frac{\beta}{1 - (\omega^2/\omega_T)^2 + \hbar^2 K^2/(M \omega_T)} \right], \quad (9.43)$$

where  $\beta$  is the oscillator strength and the energy is  $\hbar\omega_X = \hbar\omega_T + \hbar^2 K^2/2M$ .  $\hbar\omega_T$  is the energy of the transverse exciton at  $K = 0$ . With this dispersion the wave dispersion must be fulfilled, i.e.

$$c^2 k^2 = \omega^2 \epsilon(\omega), \quad (9.44)$$

where  $k$  is the  $k$ -vector of the light that needs to be  $k = K$  due to momentum conservation. The dependence of the dielectric function on  $k$  is called *spatial dispersion* [763]. Generally, up to terms in  $k^2$  it is written as

$$\epsilon(\omega) = \epsilon_b \left[ 1 + \frac{\beta}{1 - (\omega^2/\omega_0)^2 + D k^2} \right]. \quad (9.45)$$

The term  $k^2$  with curvature  $D$  (for the exciton polariton  $D = \hbar/(M\omega_T)$ ) plays a role in particular when  $\omega_T^2 - \omega^2 = 0$ . For  $\mathbf{k} \neq 0$  even a cubic material is anisotropic. The dimensionless curvature  $\hat{D} = Dk'^2$  should fulfill  $\hat{D} = \hbar/(Mc) \ll 1$  in order to make  $k^4$  terms unimportant. For exciton polaritons<sup>8</sup> typically  $\hat{D} = \hbar\omega_T/(m c^2) \approx 2 \times 10^{-5}$  for  $\hbar\omega_T = 1$  eV and  $m^* = 0.1$ .

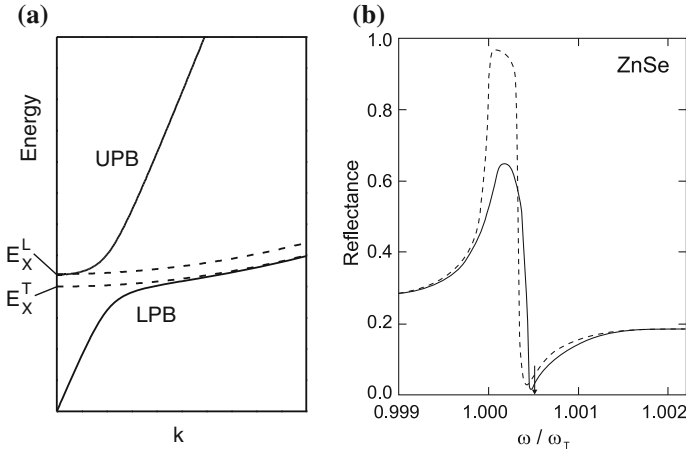


**Fig. 9.22** (a) Schematic dispersion of exciton polaritons. The lower polariton branch ('LPB') is at small  $k$  photon-like, at large  $k$  exciton-like. The upper branch ('UPB') is exciton-like at small  $k$  and photon-like at larger  $k$ . The limit of the UPB for  $k \rightarrow 0$  is the energy of the longitudinal exciton. The *dashed lines* represent the pure exciton dispersions. (b) Theoretical effect of spatial dispersion on the reflectance at the fundamental exciton resonance at normal incidence for ZnSe material parameters ( $\hbar\omega_T = 2.8$  eV,  $\beta = 1.0 \times 10^{-3}$  and a background dielectric constant of  $\epsilon_b = 8.1$ , damping was set to  $\Gamma = 10^{-5}\omega_T$ ). The *arrow* denotes the position of  $\omega_L$ . The *solid (dashed) line* is with (without) spatial dispersion for  $\hat{D} = 0.6 \times 10^{-5}$  ( $\hat{D} = 0$ ). Data from [763]

From (9.44) together with (9.45) two solutions result:

$$2\omega^2 = c^2k^2 + (1 + \beta + Dk^2)\omega_0^2 \pm \left[ -4c^2k^2(1 + Dk^2)\omega_0^2 + (c^2k^2 + (1 + \beta + Dk^2)\omega_0^2)^2 \right]^{1/2}. \quad (9.46)$$

The two branches are shown schematically in Fig. 9.22a. Depending on the  $k$  value they have a photonic (linear dispersion) or excitonic (quadratic dispersion) character. The anticrossing behavior at  $k' \approx \omega_T/c$  (for  $\hbar\omega_T = 1$  eV,  $k' \approx 0.5 \times 10^{-5} \text{ cm}^{-1}$ ) creates a bottleneck region in the lower polariton branch. This name stems from the small emission rate of acoustic phonons (i.e. cooling) in that region, as predicted in [764] and experimentally found, e.g. in CdS [765]. The polaritons decay into a

<sup>8</sup>The dependence of the optical-phonon energies on  $k$  is typically too small to make spatial dispersion effects important. According to (5.19)  $\hat{D} = -(a_0\omega_{\text{TO}}/4c)^2 \approx 4 \times 10^{-11}$  for typical material parameters (lattice constant  $a_0 = 0.5$  nm, TO phonon frequency  $\omega_{\text{TO}} = 15$  THz).

photon when they hit the surface. The effect of the oscillator strength of the dispersion is shown in Fig. 9.23 for two-exciton resonance. In the case of several excitons (9.45) reads

$$\epsilon(\omega) = \epsilon_b \left[ 1 + \sum_{i=1}^n \frac{\beta_i}{1 - (\omega^2/\omega_{0,i})^2 + D_i k^2} \right]. \quad (9.47)$$

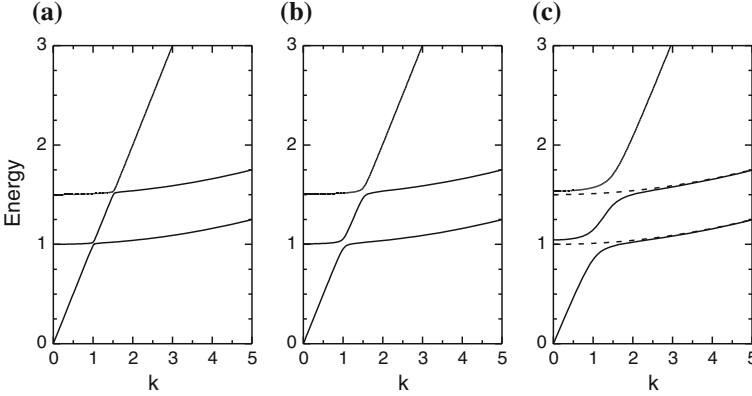


**Fig. 9.23** Schematic polariton dispersion for a two-exciton resonance (curvature of exciton dispersion greatly exaggerated,  $\hat{D} = 10^{-2}$ ) at  $\omega_{T,1} = 1$  and  $\omega_{T,2} = 1.5$  for three different oscillator strengths (a)  $f = 10^{-3}$ , (b)  $f = 10^{-2}$ , (c)  $f = 10^{-1}$ . The dashed lines in (c) represent the pure exciton dispersions

For  $k = 0$  either  $\omega = 0$  (lower polariton branch) or  $\epsilon(\omega_L) = 0$ . For the latter we find from (9.45)

$$\omega_L = \sqrt{1 + \beta} \omega_T. \quad (9.48)$$

Therefore, the energy splitting  $\Delta E_{LT}$ , mostly denoted as  $\Delta_{LT}$ , between the L- and T-exciton energy given by

$$\Delta E_{LT} = \hbar(\omega_L - \omega_T) = \left[ \sqrt{1 + \beta} - 1 \right] \hbar\omega_T \approx \frac{1}{2} \beta \hbar\omega_T \quad (9.49)$$

is proportional to the exciton oscillator strength (for experimental values see Table 9.6). We note that if (D.9) is used for the dielectric function,  $\beta$  in (9.49) needs to be replaced by  $\beta/\epsilon_b$ .

The effect of spatial dispersion on the reflection at the fundamental exciton resonance is depicted in Fig. 9.22b. For non-normal incidence an additional feature due to the longitudinal wave is observed for p-polarization [763]. For a detailed discussion additional effects due to anisotropy in wurtzite crystals, an exciton free layer at the semiconductor surface, additional boundary conditions and damping need to

**Table 9.6** Exciton energy (low temperature), LT splitting and exciton polariton oscillator strength for various semiconductors

	CdS A	CdS B	ZnO A	ZnO B	ZnSe	GaN A	GaN B	GaAs
$\hbar\omega_T$ (eV)	2.5528	2.5681	3.3776	3.3856	2.8019	3.4771	3.4816	1.5153
$\Delta_{LT}$ (meV)	2.2	1.4	1.45	5	1.45	1.06	0.94	0.08
$\beta$ ( $10^{-3}$ )	1.7	1.1	0.9	3.0	1.0	0.6	0.5	0.11

Values for ZnO from [766], values for GaAs from [767], all other values from [768]

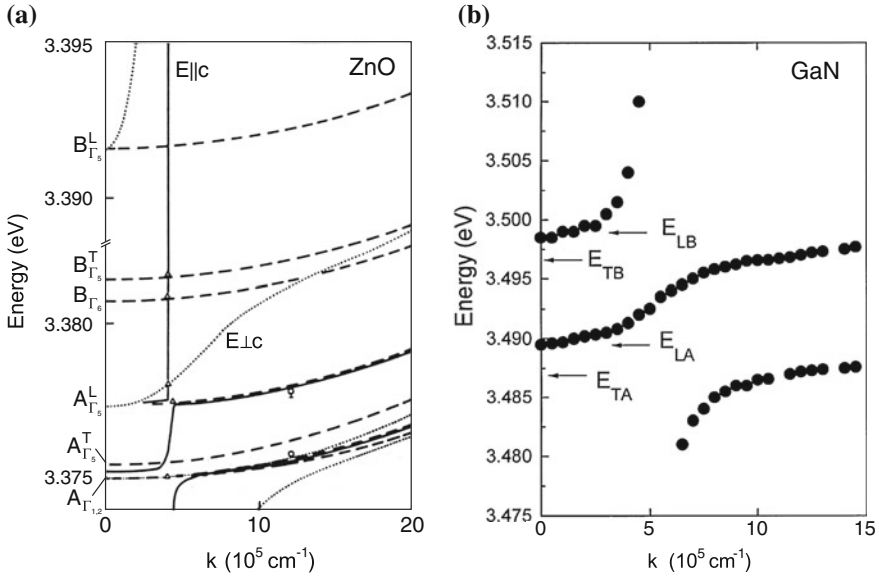


**Fig. 9.24** (a) Exciton polariton dispersion ( $\mathbf{k} \perp c$ ) of ZnO with experimental data ( $T = 1.8$  K). Solid (dotted) lines are for polaritons with  $\mathbf{E} \parallel c$  ( $\mathbf{E} \perp c$ ). The dashed lines refer to excitons. Adapted from [771]. (b) Exciton polariton dispersion ( $T = 2$  K) in GaN (on sapphire) for  $\mathbf{E} \perp c$ . Adapted from [772]

be considered [769, 770]. The polariton dispersions of ZnO and GaN are shown in Fig. 9.24.

### 9.6.9 Bound-Exciton Absorption

Excitons can localize at impurities or inhomogeneities. Such excitons are called *bound excitons*. Here, the absorption due to such complexes is discussed. The recombination is discussed in Sect. 10.3.2. In GaP:N excitons are bound to isoelectronic

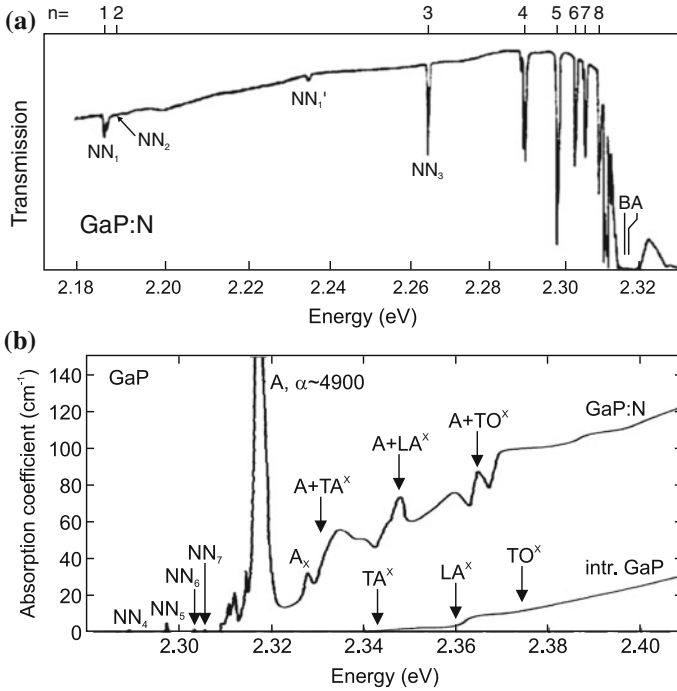


**Fig. 9.25** (a) Transmission spectrum of GaP:N with a nitrogen concentration of about  $10^{19} \text{ cm}^{-3}$  at 1.6 K (thickness: 1.1 mm).  $n$  is indicated for the first eight transitions due to excitons bound to nitrogen pairs.  $NN_n$  indicate phonon replica. The ‘A’ line denotes the position of the transition due to excitons bound to a single nitrogen atom (observable for samples with low N doping). The ‘B’ line is forbidden and due to the  $J = 2$  exciton. Adapted from [616]. (b) Absorption spectra of N-doped ( $N_N = 7 \times 10^{18} \text{ cm}^{-3}$ ) and intrinsic GaP ( $T = 2 \text{ K}$ ). Adapted from [612]

N impurities (substituting P), resulting in the ‘A’ line at 2.3171 eV (at  $T = 4.2 \text{ K}$ ).<sup>9</sup> The absorption due to A excitons is well resolved in the spectrum of Fig. 9.25b. At sufficiently high nitrogen doping, there exist nitrogen pairs, i.e. a complex where a nitrogen impurity has a second nitrogen impurity in the vicinity. The pairs are labeled  $NN_n$ . It was believed that the second nitrogen atom is in the  $n$ -th shell around the first one. However, the proper level assignment is probably different in the view of modern theory [472]. Also clusters with more than two nitrogen atoms may exist.  $NN_1$  is a prominent level and relates to a N–Ga–N complex having 12 equivalent sites for the second N atom on the next neighbor anion site. The transitions due to excitons bound to  $NN_n$ , as shown in Fig. 9.25a, give a series of lines (see Table 9.7) that fulfill  $\lim_{n \rightarrow \infty} NN_n = A$ . Although GaP has an indirect band structure, the absorption coefficient of N-related transitions is large, about  $10^5 \text{ cm}^{-1}$  for a nitrogen doping

<sup>9</sup>The A line is due to excitons with  $J = 1$ , resulting of coupling of the electron spin 1/2 with the hole angular momentum of 3/2. The B-line is a dipole forbidden line due to ‘dark’ excitons with  $J = 2$ .

**Table 9.7** Index of nitrogen pairs  $NN_n$  and energy separation  $\Delta E$  of bound-exciton transitions from the free-exciton line for  $n = 1 \dots 10$  and the ‘A’ line

$n$	1	2	3	4	5	6	7	8	9	10	$\infty$ (A)
$\Delta E$ (meV)	143	138	64	39	31	25	22	20	18	17	11

level of  $10^{19} \text{ cm}^{-3}$ .<sup>10</sup> This is due to the fact that the electron spatially localized at the nitrogen isoelectronic trap (Sect. 7.7.9) has a sizeable  $k = 0$ -component of its wave-function (Fig. 7.41), leading to a large transition probability for  $\Gamma$ -point holes with an oscillator strength of 0.09 [773].

### 9.6.10 Biexcitons

Similar to two hydrogen atoms forming a hydrogen molecule, two excitons can also form a bound complex, the biexciton involving two electrons and two holes. The biexciton binding energy is defined as

$$E_{XX}^b = 2 E_X - E_{XX}. \tag{9.50}$$

Biexcitons are binding in bulk material. Accordingly, the biexciton recombination or absorption occurs at lower energy than that of the exciton. Values of the biexciton binding energy are listed in Table 9.4 for various semiconductors. The ratio of biexciton and exciton binding energies is fairly constant about 0.2. In semiconductors with small exciton binding energy, such as GaAs, biexcitons are hard to observe in bulk material but show up in heterostructures that provide additional carrier confinement (see also Sect. 14.3.4). While the exciton density increases linearly with external excitation, the density of biexcitons increases quadratically.

### 9.6.11 Trions

The complexes ‘ehh’ and ‘ehh’ are called trions. Also, the notation  $X^-$  and  $X^+$  is common.  $X^-$  is typically stable in bulk material but hard to observe. In quantum wells or dots, trions are easier to observe. In quantum dots excitons with higher charge, e.g.  $X^{2-}$ , have also been observed (see Fig. 14.34).

---

<sup>10</sup>Also the recombination (Sect. 10.3.2) is efficient and allows green GaP:N and yellow GaAsP:N light emitting diodes.

### 9.6.12 Band Gap Renormalization

The band structure theory has been developed so far for small carrier densities. If the carrier density is large the interaction of free carriers has to be considered. The first step was exciton formation. However, at high temperatures (ionization) and at large carrier density (screening) the exciton is not stable. Exchange and correlation energy leads to a decrease of the optical absorption edge that is called *band gap renormalization* (BGR).

An effect due to significant carrier density is to be expected when the density is of the order of the exciton volume, i.e.  $n \sim a_B^{-3}$ . For  $a_B \sim 15 \text{ nm}$  (GaAs) this means  $n \sim 3 \times 10^{17} \text{ cm}^{-3}$ . The dimensionless radius  $r_s$  is defined via

$$\frac{4\pi}{3} r_s^3 = \frac{1}{n a_B^3}. \tag{9.51}$$

The sum of exchange and correlation energies  $E_{xc}$  is found to be mostly independent of material parameters [774] (Fig. 9.26a) and follows the form

$$E_{xc} = \frac{a + b r_s}{c + d r_s + r_s^2}, \tag{9.52}$$

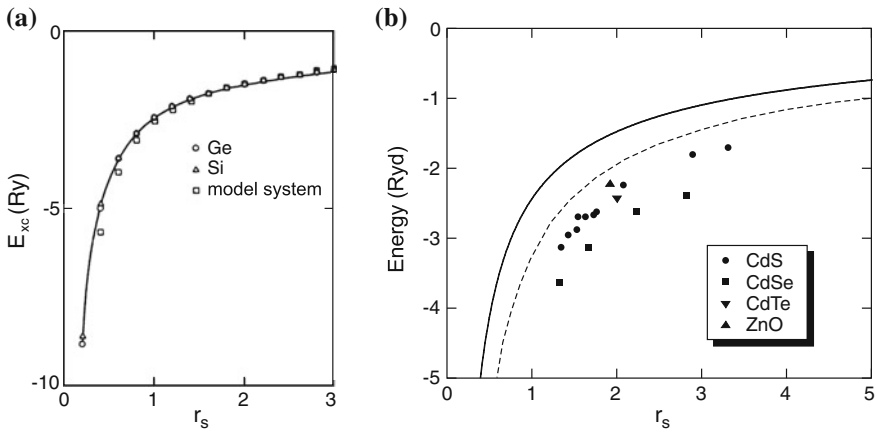
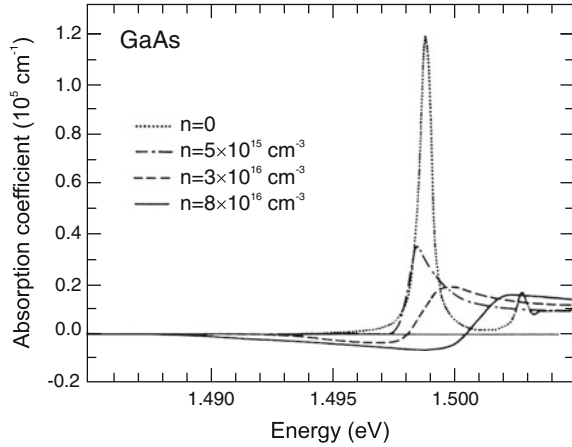


**Fig. 9.26** (a) Theoretical exchange and correlation energies in units of the exciton Rydberg energy as a function of the dimensionless variable  $r_s$  for Ge, Si and a model system (with one isotropic conduction and valence band each). The *solid line* is a fit according to (9.52). Adapted from [774]. (b) Band gap renormalization in terms of the excitonic Rydberg for various II–VI semiconductors. *Solid line* is the relation according to (9.52), *dashed line* is the dependence predicted in [775] for  $T = 30 \text{ K}$ . Data are compiled in [776]

**Fig. 9.27** Absorption of GaAs (low temperature,  $T = 10\text{K}$ ) as a function of the electron–hole density  $n$  (theory). Adapted from [777]



with  $a = -4.8316$ ,  $b = -5.0879$ ,  $c = 0.0152$  and  $d = 3.0426$ . Thus the density dependence of the band gap at small carrier density is  $\propto n^{1/3}$ . Experimental data for a number of II–VI semiconductors roughly follow such a dependence (Fig. 9.26b).

In Fig. 9.27, a theoretical calculation of the absorption spectrum of bulk GaAs for various carrier densities ( $n = p$ ) [777] is shown. With increasing density, the excitonic resonance broadens and vanishes. The shape approaches the electron–hole plasma shape. The absorption edge shifts to smaller energies. At high carrier density, the absorption becomes negative in a spectral range before absorption sets in. In this spectral region, the material exhibits gain and an incoming light wave is amplified (cmp. Sect. 10.2.6).

### 9.6.13 Electron–Hole Droplets

At low temperature and high density, electron–hole pairs in Ge and Si can undergo a phase transition into a liquid state. This electron–hole liquid (EHL) was suggested in [778] and is a Fermi liquid exhibiting the high conductivity of a metal and the surface and density of a liquid. The condensation is due to exchange interaction and correlation. The formation is fostered by the band structure of Ge [779] and the long lifetime of carriers in the indirect band structure. In unstressed Ge typically a cloud of electron–hole droplets with diameter in the  $\mu\text{m}$  range exists. The phase diagram is shown in Fig. 9.28a. In suitably stressed Ge electron–hole droplets with several hundred  $\mu\text{m}$  diameter form around the point of maximum shear strain in inhomogeneously strained crystals, as shown in Fig. 9.28b. The pair density in such a liquid is of the order of  $10^{17}\text{cm}^{-3}$ .

We note that the metallic EHL state hinders observation of the Bose–Einstein condensation (BEC) of (bosonic) excitons. The light-exciton mass offers a high

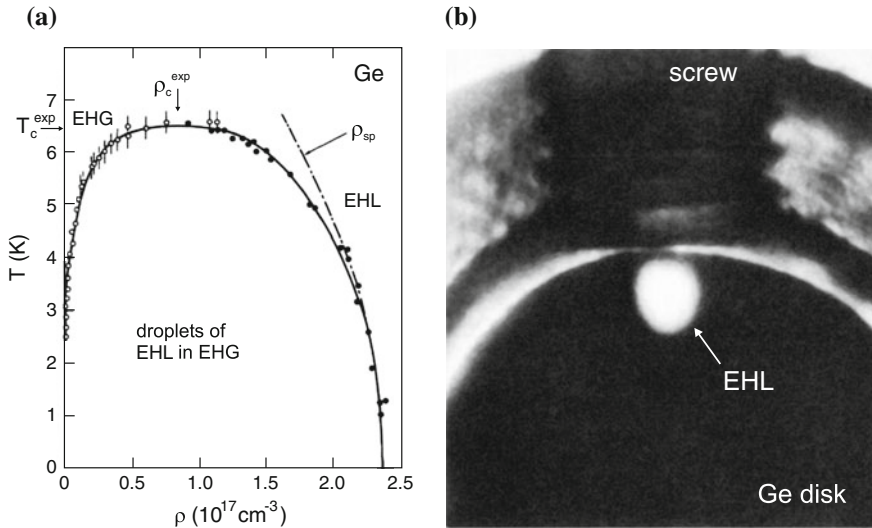


**Fig. 9.28** (a) Temperature–density phase diagram of electrons and holes in Ge. The regions of electron–hole gas (EHG) and liquid (EHL) and the droplet phase are labeled. *Solid line* is theoretical calculation, *symbols* are experimental data from [780]. The *dash-dotted line* denoted  $\rho_{sp}$  is the experimentally obtained temperature dependence of the liquid density due to single-particle excitations.  $\rho_c^{exp}$  and  $T_c^{exp}$  denote the experimental critical density and temperature, respectively. Adapted from [781]. (b) Photographic image of radiative recombination (at  $1.75\ \mu\text{m}$  wavelength) from a  $300\text{-}\mu\text{m}$  diameter droplet of electron–hole liquid (EHL) in a stressed (001) Ge disk (diameter 4 mm, thickness 1.8 mm) at  $T = 2\ \text{K}$ . The stress is applied from the top by a nylon screw along a (110) direction. Adapted from [782], reprinted with permission, © 1977 APS

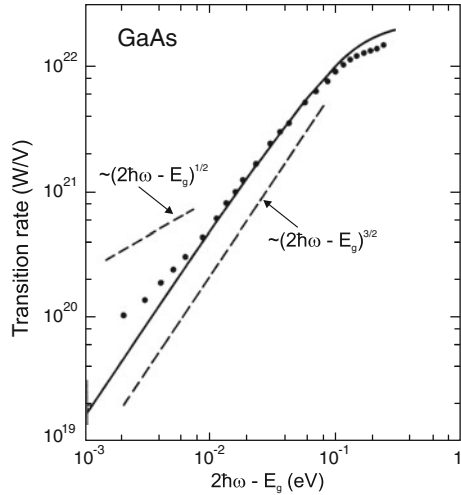
condensation temperature in the 1 K range (compared to the mK range for atoms). Recent experiments with spatially indirect excitons in coupled quantum wells lead towards BEC [783, 784]. A sufficiently long lifetime ensures cooling of the excitons close to the lattice temperature. Another potential candidate for BEC are long-living excitons (ms-range) in  $\text{Cu}_2\text{O}$  [785]. The condensation of polaritons (cf. Sect. 9.6.8) in microcavities to well-defined regions of  $\mathbf{k}$ -space has been discussed in [786] and compared to bosonic condensation in bulk.

### 9.6.14 Two-Photon Absorption

So far, only absorption processes that involve one photon have been considered. The attenuation of the intensity  $I$  of a light beam (of frequency  $\omega_0$ ) along the  $z$  direction can be written as

$$\frac{dI}{dz} = -\alpha I - \beta I^2, \quad (9.53)$$

**Fig. 9.29** Experimental two-photon absorption spectrum of GaAs ( $T = 4\text{ K}$ ) (dots) plotted as a function of the difference of the double-photon energy  $2\hbar\omega$  from the GaAs band edge  $E_g$ . The solid line is a theoretical calculation, the dashed lines represent slopes with exponent  $1/2$  and  $3/2$ , respectively. Adapted from [789]



where  $\alpha$  is due to the (linear) absorption coefficient (and possibly scattering) and  $\beta$  is the two-photon absorption coefficient. A two-photon process can occur in two steps, e.g. via a midgap level, which is not considered any further here. Here, we consider two-photon absorption (TPA) via the population of a state at  $2\hbar\omega_0$  higher energy than the initial state with a nonlinear optical process. The TPA coefficient is related to the nonlinear third-order electric dipole susceptibility tensor [787]  $\chi_{ijkl}$ . Within the two-band approximation theory predicts [788]

$$\beta \propto (2\hbar\omega_0 - E_g)^{3/2}. \tag{9.54}$$

The exponent  $3/2$  is indeed found experimentally, as shown in Fig. 9.29 for GaAs. The strength of absorption depends on the relative orientation of the light polarization with respect to the main crystallographic directions, e.g. TPA for polarization along  $\langle 110 \rangle$  is about 20% larger than for the  $\langle 100 \rangle$  orientation.

## 9.7 Impurity Absorption

### 9.7.1 Shallow Levels

For charge carriers bound to shallow impurities long range Coulomb forces are most important and they exhibit a hydrogen-like term scheme

$$E_n = \frac{m^*}{m_0} \frac{1}{\epsilon_r^2} \frac{1}{n^2} \times 13.6\text{ eV}, \tag{9.55}$$

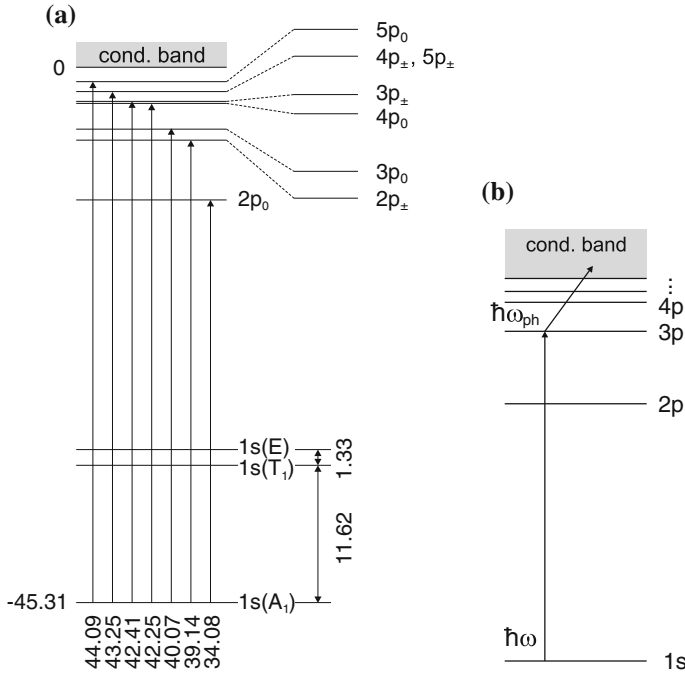


**Fig. 9.30** (a) Term scheme of phosphorus donor in silicon, all energies in meV. After [791]. (b) Schematic sequence for photothermal ionization, here absorption of a photon with  $\hbar\omega = E_{3p} - E_{1s}$  and subsequent absorption of a phonon with energy  $\hbar\omega_{ph} \geq E_{\infty} - E_{3p}$

with the ionization limit  $E_{\infty}$  being the conduction (valence) band edge for donors (acceptors), respectively. They can be excited by light to the nearest band edge. Such absorption is typically in the FIR region and can be used for photodetectors in this wavelength regime. The optical absorption cross section of impurity absorption can be related to the carrier capture cross section [513, 514].

The actual transition energies can deviate from (9.55) due to deviation of the potential close to the impurity from the pure Coulomb potential. Such an effect is known as the chemical shift or central cell correction (cf. Sect. 7.5.5) and is characteristic of the particular impurity. In GaAs such shifts are small ( $\sim 100 \mu\text{eV}$ ) [790].

The term scheme for P in Si is shown in Fig. 9.30a. The ground state ( $1s$ ) is split because of a reduction of the tetrahedral symmetry due to intervalley coupling. The anisotropic mass at the X-valley in Si causes the  $p$  states (and states with higher orbital momentum) to split into  $p_0$  and  $p_{\pm}$  states. Such an effect is absent in a direct semiconductor with an isotropic conduction-band minimum such as GaAs (Fig. 9.31). Optical transitions between the  $1s$  and various  $p$  states can be directly observed in absorption, e.g. for Si:P [792]. These transitions are also observed in photoconductivity because the missing energy to the ionization into the continuum is supplied by a phonon at finite temperature (photothermal ionization) (Fig. 9.30b) [791]. The

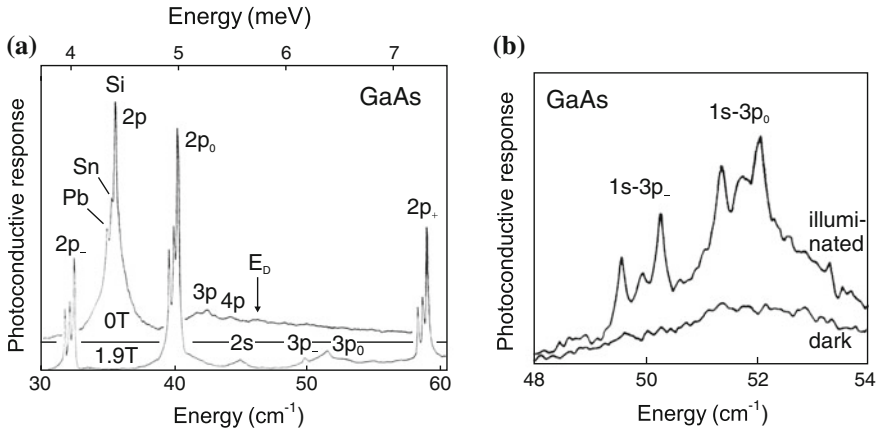


**Fig. 9.31** (a) Far-infrared photoconductivity response (Lyman-type  $s \rightarrow p$  series) of not intentionally doped GaAs with residual donors Pb, Sn, and Si,  $N_A = 2.6 \times 10^{13} \text{ cm}^{-3}$ ,  $N_D - N_A = 8 \times 10^{12} \text{ cm}^{-3}$ . The upper (lower) curve is for a magnetic field of 0 (1.9) T. Measurement temperature is 4.2 K. (b) Photoconductive response of a (different) GaAs sample with the same impurities ( $N_D = 1 \times 10^{13} \text{ cm}^{-3}$ ) with (upper curve) and without (lower curve) illumination with above-bandgap light ( $B = 1.9 \text{ T}$ ,  $T = 4.2 \text{ K}$ ). Adapted from [793]

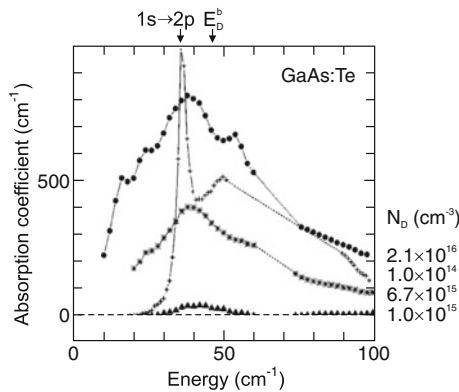


**Fig. 9.32** Low-temperature ( $T = 1.35 \text{ K}$ ) absorption spectra of highly doped n-type GaAs:Te with doping concentrations as labeled (circles  $N_D = 2.1 \times 10^{16} \text{ cm}^{-3}$ , stars  $6.7 \times 10^{14}$ , triangles  $1.0 \times 10^{15}$ ). A sharp photoconductivity spectrum (in arbitrary units) from low-doped GaAs:Te (crosses,  $N_D = 1.0 \times 10^{14} \text{ cm}^{-3}$ ) is shown for comparison (cf. Fig. 9.31a). The energy of the  $1s \rightarrow 2p$  transition and the donor binding energy (onset of continuum absorption) are indicated. Adapted from [794]

splitting of the  $2p$  transition in Fig. 9.31a is the chemical shift due to different donors incorporated in the GaAs (Si, Sn, and Pb). Peak broadening is mostly due to Stark broadening due to neighboring charged impurities. The application of a magnetic field induces Zeeman-like splittings and increases the sharpness of the peaks. The peak width can be further increased by illuminating the sample with light having a

higher energy than the band gap. The additional charge carriers neutralize charged impurities and allow higher resolution (Fig. 9.31b).

In Fig. 9.32 absorption spectra of highly doped n-type GaAs are shown. For doping concentrations larger than the critical concentration of  $\sim 1 \times 10^{16} \text{ cm}^{-3}$  (cf. Table 7.6) significant broadening is observed due to the formation of an impurity band.

### 9.7.2 Deep Levels

The absorption of deep levels is typically in the infrared. In Fig. 9.33a the possible optical absorption processes involving the Fe levels in InP (cf. Sect. 7.7.8) during the charge transfer  $\text{Fe}^{3+} \rightarrow \text{Fe}^{2+}$  are shown. These transitions and their fine structure (Fig. 9.33b) have been observed in calorimetric absorption spectroscopy (CAS) experiments [604].

In Fig. 9.34 the photoconductivity of is shown. The sharp peaks are due to transitions of interstitial, singly ionized Mg,  $\text{Mg}_i^+$  [795]. Mg in Si is a double donor [575] (see Sect. 7.7.2). Above the ionization limit of about 256 meV, the peaks are replicated, shifted by the LO phonon energy of 59.1 meV. However, now they rather appear as dips. This behavior is typical for a discrete state interacting with a continuum, also called Fano resonance [796, 797] with its characteristic lineshape, going *below* the continuum level.

The absorption spectra due to various deep acceptors in GaAs are compared in Fig. 9.35. The density of states in the band increases with  $k$  (proportional to  $\sqrt{E - E_c}$ ). The carrier on the impurity is strongly localized and described with a wave packet centered around  $\Gamma$ , its  $k$ -components decreasing with increasing  $k$ . Thus the maximum absorption will be at an intermediate  $k$ -value and an associ-

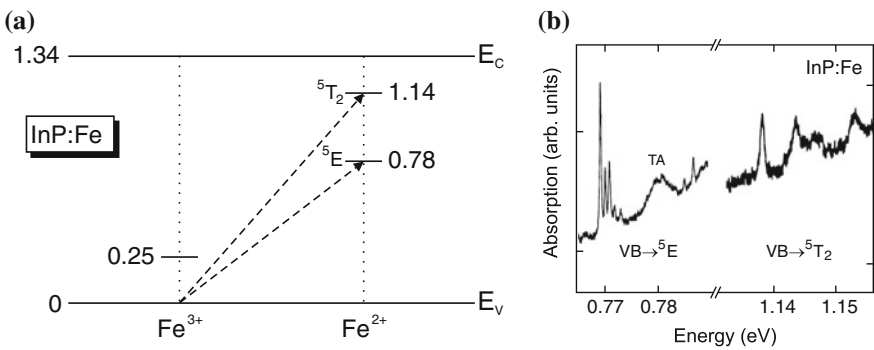


**Fig. 9.33** (a) Schematic band diagram of InP with levels of Fe impurities in the 3+ and 2+ charge states at low temperature. All energies are given in eV. The *arrows* denote the optical transition of a valence-band electron to the Fe center,  $\text{Fe}^{3+} + \hbar\omega \rightarrow \text{Fe}^{2+} + h$ . (b) Calorimetric absorption spectra (at  $T = 1.3 \text{ K}$ ) of InP:Fe,  $[\text{Fe}] = 5 \times 10^{16} \text{ cm}^{-3}$ . Part (b) adapted from [604]

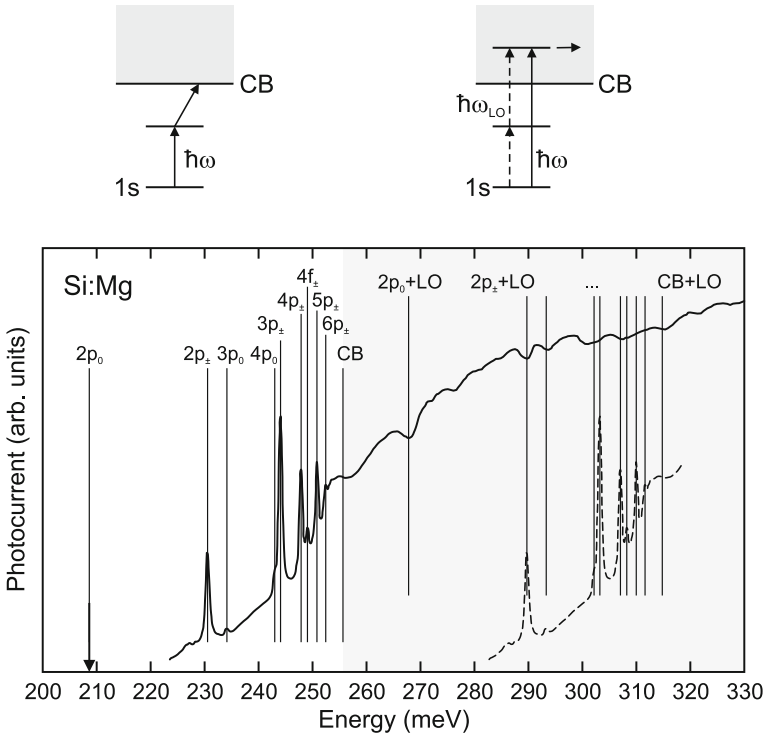
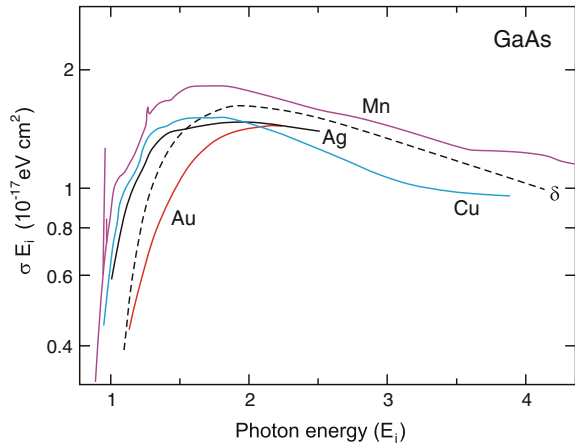


**Fig. 9.34** Photocurrent spectrum of Si:Mg. Transitions are due to  $Mg_i^+$  from its  $1s$  state to excited states as labeled and indicated by vertical lines. CB denotes the conduction band edge (ionization limit). Above the CB edge (shaded area) phonon-assisted absorption occurs (Fano resonances). For comparison the absorption spectrum below CB is shown shifted by the phonon energy (dashed line). Above the plot, the transition mechanisms (photothermal ionization and Fano resonance) are schematically shown. Adapted from [795]

**Fig. 9.35** Absorption spectra ( $\sigma = \alpha/p$ ) due to various deep impurities in GaAs as labeled. The dashed line is a theoretical lineshape assuming a hole bound to a  $\delta$ -potential. The energy axis is scaled by the ionization energy. The kink for Mn at  $3.5 E_i \approx 450 \text{ meV}$  is due to the onset of absorption into the split-off valence band. Adapted from [279]



ated energy larger than the ionization energy  $E_i$  (lowest transition to continuum at for  $k = 0$ ). The lineshapes in Fig. 9.35 fit to a model with a  $\delta$ -potential (zero range model, neglecting long range Coulomb terms) [798] with maximum absorption close to  $2 E_i$ ,

$$\alpha(E) \propto \frac{E_i^{1/2} (E - E_i)^{3/2}}{E^3}. \quad (9.56)$$

## 9.8 Absorption in the Presence of Free Charge Carriers

In the presence of charge carriers, various absorption processes can occur. First, the dissipative motion of carriers leads to infrared absorption, termed the free carrier absorption (Sect. 9.8.1). Filling of a band with carriers leads to a shift of the band-band absorption edge, the Burstein–Moss shift (Sect. 9.8.2). Besides the free-carrier absorption, free carriers present in the semiconductor can lead to further absorption processes with transition energies below the band gap. These processes are due to transitions within the band structure and can be

- inter-valence band transitions of holes (Sect. 9.8.3),
- phonon-assisted inter-valley transitions of electrons (Sect. 9.8.4),
- phonon-assisted intra-band transitions of electrons (Sect. 9.8.5).

### 9.8.1 Free-Carrier Absorption

The absorption due to free carriers in the infrared spectral range (away from phonon resonances) can be described with the Drude model [799].

A time-dependent electric field accelerates the charge carriers within a band. The excess energy is subsequently transferred to the lattice via scattering with phonons. A review of the effect of free carriers on optical properties can be found in [800]. In the relaxation-time approximation energy is relaxed with a time constant  $\tau$ . Thus energy is absorbed from the electromagnetic wave and dissipated. Effectively, this process represents an intra-band excitation.

The complex conductivity (8.36) is given by

$$\sigma^* = \sigma_r + i\sigma_i = \frac{n e^2 \tau}{m^*} \left( \frac{1}{1 + \omega^2 \tau^2} + i \frac{\omega \tau}{1 + \omega^2 \tau^2} \right). \quad (9.57)$$

We note that a static magnetic field introduces birefringence as discussed in more detail in Sect. 13.2.2. The wave equation for the electric field is

$$\nabla^2 \mathbf{E} = \epsilon_r \epsilon_0 \mu_0 \ddot{\mathbf{E}} + \sigma^* \mu_0 \dot{\mathbf{E}}. \quad (9.58)$$

For a plane wave  $\propto \exp[i(\mathbf{k}\mathbf{r} - \omega t)]$  the wavevector obeys

$$k = \frac{\omega}{c} \sqrt{\epsilon_r + i \frac{\sigma^*}{\epsilon_0 \omega}}, \quad (9.59)$$

where  $c = (\epsilon_0 \mu_0)^{-1/2}$  is the velocity of light in vacuum,  $\epsilon_r$  is the background dielectric constant (for large  $\omega$ ).

The part  $\epsilon_{\text{FC}}$  of the dielectric function due to free carriers is

$$\epsilon_{\text{FC}} = \frac{i}{\epsilon_0 \omega} \sigma^*. \quad (9.60)$$

The complex index of refraction is

$$n^* = n_r + i\kappa = \sqrt{\epsilon_r + i \frac{\sigma^*}{\epsilon_0 \omega}}. \quad (9.61)$$

Taking the square of this equation yields

$$n_r^2 - \kappa^2 = \epsilon_r + i \frac{\sigma_i}{\epsilon_0 \omega} = \epsilon_r - \frac{n e^2}{\epsilon_0 m^*} \frac{\tau^2}{1 + \omega^2 \tau^2} \quad (9.62a)$$

$$2 n_r \kappa = \frac{\sigma_r}{\epsilon_0 \omega} = \frac{n e^2}{\epsilon_0 \omega m^*} \frac{\tau}{1 + \omega^2 \tau^2}. \quad (9.62b)$$

The absorption coefficient is related to  $\kappa$  by (9.9). For the case of higher frequencies, i.e.  $\omega\tau \gg 1$ , the absorption is

$$\alpha = \frac{n e^2}{\epsilon_0 c n_r m^* \tau} \frac{1}{\omega^2}. \quad (9.63)$$

The absorption decreases with increasing frequency like  $\omega^{-r}$ . The classical Drude treatment as followed here results in an exponent of  $r = 2$ . This is the case for neutral impurity scattering and also for small frequencies  $\hbar\omega \ll E_F$ . A more detailed discussion of the energy dependence of free-carrier absorption can be found in [801]. Other exponents have been derived for scattering by acoustical phonons ( $r = 3/2$ ), LO phonons ( $r = 5/2$ ) and ionized impurities ( $r = 7/2$ ). More detailed quantum mechanical treatments of free-carrier absorption in the presence of impurities and phonons can be found in [802, 803].

For semiconductors free-carrier absorption is particularly important in the mid- and far-infrared regions when carriers are present due to doping or thermal excitation. In Fig. 9.36a absorption spectra of n-type Ge for various doping concentrations are shown. The absorption coefficient in the transparency regime varies proportionally to  $\lambda^2 \propto \omega^{-2}$  as predicted in (9.63). In Fig. 9.36a, the absorption can be seen to rise for photon energy above 0.7 eV due to absorption in the band structure. Electrons are

excited from the valence band across the fundamental band gap into the conduction band (cmp. Sect. 9.6.3), which is an indirect transition in Ge.

In Fig. 9.36b the absorption coefficient due to free carrier absorption at fixed wavelength is shown as a function of dopant concentration.<sup>11</sup> The slope is slightly overlinear, indicating a weak dependence  $\tau(n)$ . A sub-linear relation has been found for heavily p-doped GaAs [804].

The index of refraction is given by (also for  $\omega\tau \gg 1$ )

$$n_r^2 = \epsilon_r - \frac{ne^2}{\epsilon_0 m^* \omega^2} + \kappa^2 = \epsilon_r \left[ 1 - \left( \frac{\omega_p}{\omega} \right)^2 \right] + \frac{\epsilon_r^2}{4n_r^2} \left( \frac{\omega_p}{\omega} \right)^4 \frac{1}{\omega^2 \tau^2}$$

$$\approx \epsilon_r \left[ 1 - \left( \frac{\omega_p}{\omega} \right)^2 \right], \tag{9.64}$$

where

$$\omega_p = \sqrt{\frac{ne^2}{\epsilon_r \epsilon_0 m^*}} \tag{9.65}$$

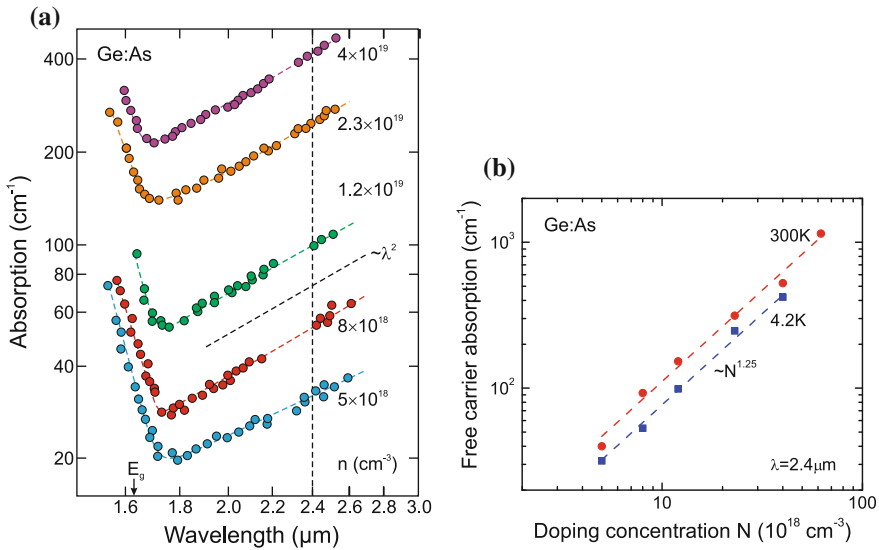


**Fig. 9.36** (a) Optical absorption spectra (at  $T = 4.2\text{K}$ ) of n-type Ge for various As dopant concentrations as labeled. The arrow denotes the band edge of undoped Ge, the vertical dashed line the energy for which the free-carrier absorption is measured in part (b). The inclined dashed line visualizes the slope  $\propto \lambda^2$ . Curved dashed lines are guides to the eye. Adapted from [739]. (b) Free-carrier absorption at  $\lambda = 2.4\ \mu\text{m}$  as determined from part (a) of the figure (blue squares) as a function of As dopant concentration. Additionally data at 300K (red circles) from the same samples are included [739]. The dashed lines visualizes the slope  $\propto N_D^{1.25}$

<sup>11</sup>Even at low temperature,  $n \approx N_D$  since  $N_D \gg N_c$  (cf. [515] and Sect. 7.5.7).

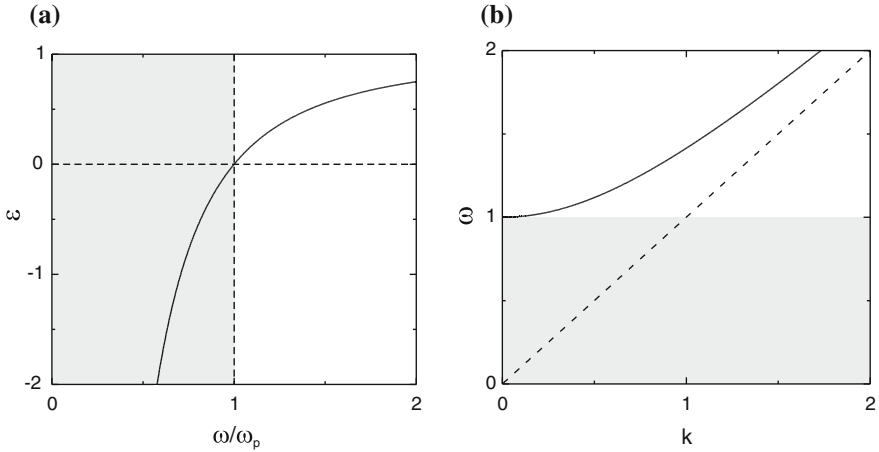
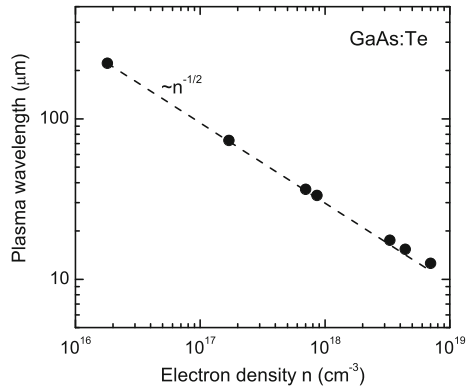


**Fig. 9.37** (a) Dielectric constant for plasmon oscillations. *Shaded area* represents region of attenuation (negative  $\epsilon$ ). (b) Dispersion relation ( $k$  in units of  $\omega_p/c$ ,  $\omega$  in units of  $\omega_p$ ) in the presence of free carriers (9.67, for  $\epsilon_r = 1$ ). *Shaded area* represents forbidden frequency range for propagating solutions. *Dashed line* is photon dispersion  $\omega = ck$

**Fig. 9.38** Plasma wavelength  $\lambda_p$  for n-type GaAs with various electron concentrations due to different doping levels. *Filled circles*: experimental values, *dashed line*:  $n^{-1/2}$  dependence; the deviation is due to nonparabolicity of the electron mass (cf. Fig. 9.50b). Data from [805]



is the plasma frequency. The approximation is valid for small absorption and when  $(\omega\tau)^{-2}$  can be neglected. A graphical representation is given in Fig. 9.37a. For coupling to electromagnetic waves (still  $\omega\tau \gg 1$ )

$$\epsilon(\omega) = \epsilon_r \left[ 1 - \left( \frac{\omega_p}{\omega} \right)^2 \right] = \frac{c^2 k^2}{\omega^2} \tag{9.66}$$

must be fulfilled. It follows that the dispersion relation in the presence of free carriers (Fig. 9.37b) is

$$\omega^2 = \omega_p^2 + \frac{c^2 k^2}{\epsilon_r}. \tag{9.67}$$

**Fig. 9.39** Czochralski-grown  $\text{Ga}_2\text{O}_3$  crystals with different electron concentration, courtesy of Z. Galazka, IKZ Berlin



For  $\omega > \omega_p$ ,  $\epsilon > 0$ , thus waves can propagate. For  $\omega < \omega_p$ , however, the dielectric constant is negative, i.e.  $\epsilon < 0$ . For such frequencies waves are exponentially damped and cannot propagate or penetrate a layer. This effect can be used in a plasmon waveguide. The expected dependence of the plasmon wavelength on the carrier density  $\lambda_p = 2\pi c/\omega_p \propto n^{-1/2}$  is depicted in Fig. 9.38 for GaAs. For semiconductors the plasmon frequency is in the mid-or far-infrared spectral region.<sup>12</sup>

The effect of free-carrier absorption is visualized in Fig. 9.39. The blue hue of the boule with the higher electron concentration is due to free carrier absorption in the long wavelength part of the visible spectrum.

### 9.8.2 Burstein–Moss Shift

In the discussion so far it has been assumed that all target states in the conduction band are empty. In the presence of free carriers the absorption is modified by the

- change of the distribution function
- many-body effects (band gap renormalization)

The latter is discussed in the next section. For a degenerate electron distribution all states close to the conduction-band edge are populated. Thus a transition from the valence band cannot take place into such states. This shift of the absorption edge to higher energies is called the Burstein–Moss shift [806, 807]. Originally, the Burstein–Moss shift was evoked to explain the absorption shift in InSb with varying carrier concentration (Fig. 9.40).

$\mathbf{k}$ -conserving optical transitions between parabolic hole and electron bands have the dependence

$$E = E_g + \frac{\hbar^2 k^2}{2 m_e^*} + \frac{\hbar^2 k^2}{2 m_h^*} = E_g + \frac{\hbar^2 k^2}{2 m_r}, \quad (9.68)$$

<sup>12</sup>The much higher free-electron density in metals shifts the plasma frequency to the UV, explaining the reflectivity of metals in the visible and their UV transparency.

**Fig. 9.40** Burstein–Moss effect at InSb ( $E_g = 0.18\text{ eV}$ ) at room temperature. Theoretical dependence and data points for intrinsic InSb and  $5 \times 10^{18}\text{ cm}^{-3}$  n-type. Data from [806]

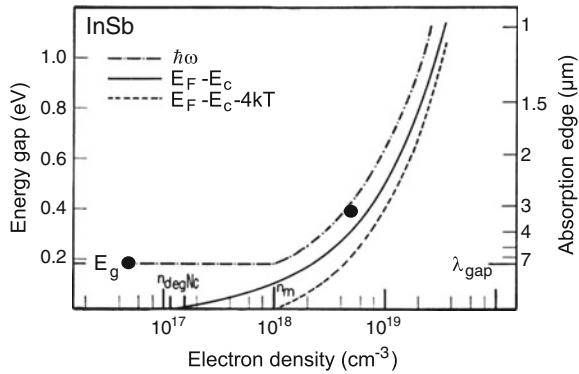
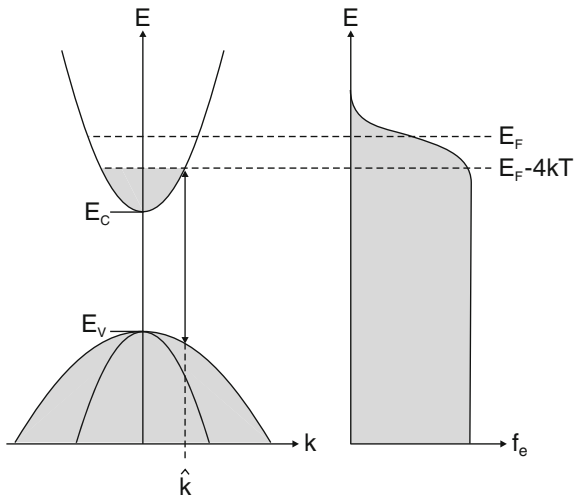


**Fig. 9.41** Principle of Burstein–Moss shift. *Left panel:* Schematic band structure with completely filled electron states shown in grey. The  $k$ -vector for the lowest photon energy optical absorption process is indicated as  $\hat{k}$ . *Right panel:* Electron distribution function for a degenerate electron gas with Fermi level in the conduction band



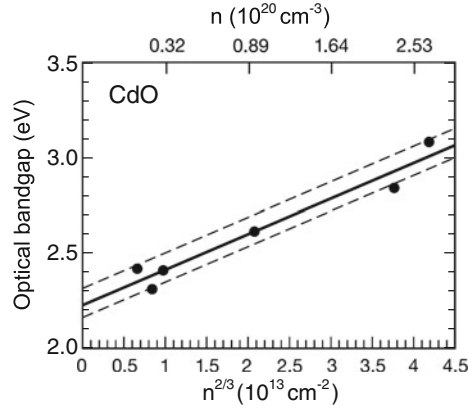
where  $m_r$  is the reduced mass of electron and hole. About  $4kT$  below the Fermi level all levels in the conduction band are populated (Fig. 9.41). Thus the  $k$  value at which the absorption starts is given as

$$\hat{k} = \sqrt{\frac{2 m_r}{\hbar^2} (E_F - E_C - 4kT)}. \tag{9.69}$$

Besides the energy shift in the conduction band, the corresponding energy shift in the valence band  $\hbar k^2/(2m_h)$  must be considered. Thus, the Burstein–Moss shift of the absorption edge is

$$\Delta E = \hbar\omega - E_g = (E_F - 4kT - E_C) \left(1 + \frac{m_e}{m_h}\right). \tag{9.70}$$

**Fig. 9.42** Burstein–Moss effect for CdO. The linear fit is for  $E_g = 2.22(8)$  eV and  $m_r = 0.113(11) m_e$ . The *dashed lines* indicate the confidence interval of  $\pm 0.08$  eV. Adapted from [808]



The relation between  $n$  and the Fermi level is given by (7.6). If  $E_F - E_C \gg kT$  the Fermi integral can be approximated by  $\frac{2}{\sqrt{\pi}} \frac{2}{3} \left( \frac{E_F - E_C}{kT} \right)^{3/2}$ . Using (7.8) for  $N_C$ , the Burstein–Moss shift can be written for this case as

$$\Delta E = n^{2/3} \frac{h^2}{8m_e} \left( \frac{3}{\pi} \right)^{2/3} \left( 1 + \frac{m_e}{m_h} \right) \approx 0.97 \frac{h^2}{8m_r} n^{2/3}. \quad (9.71)$$

The  $n^{2/3}$  dependence of the energy shift is found, e.g., for CdO<sup>13</sup> with different carrier concentrations (due to different deposition temperature, no intentional doping) [808] and depicted in Fig. 9.42.

### 9.8.3 Inter-Valenceband Transitions

Transitions within the valence band can occur between three bands, i.e. lh→hh, so→hh, and so→lh, as schematically depicted in Fig. 9.43. Theoretical treatments have been given in [809, 810]. For GaAs, such intravalence-band absorption occurs at photon energies close to  $\Delta_0$  as shown in Fig. 9.44a for p-type GaAs:Zn [811]. For p-type GaSb, the absorption coefficient below the fundamental band gap is found almost entirely due to inter-valence band transitions, as shown in Fig. 9.44b for a hole concentration of  $p = 3.2 \times 10^{16} \text{ cm}^{-3}$  [812].

<sup>13</sup>CdO is an indirect semiconductor, the optical band gap is the energy of the direct transition at the  $\Gamma$ -point. The indirect transitions involve holes from other points in the Brillouin zone (cmp. Fig. 6.10).

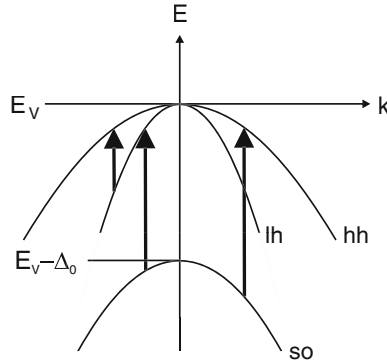


Fig. 9.43 Schematic optical transitions within the valence band

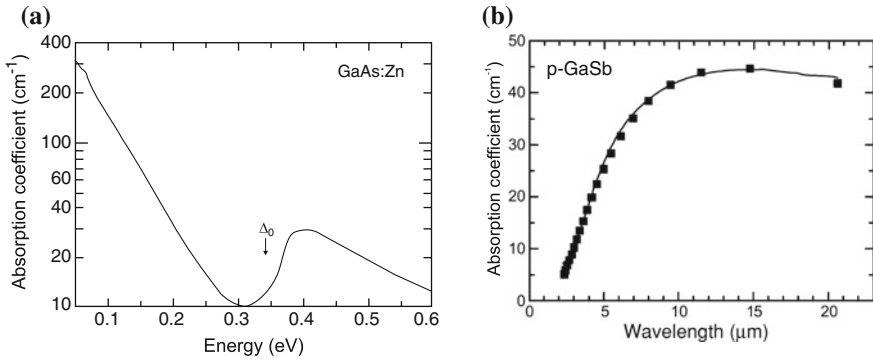
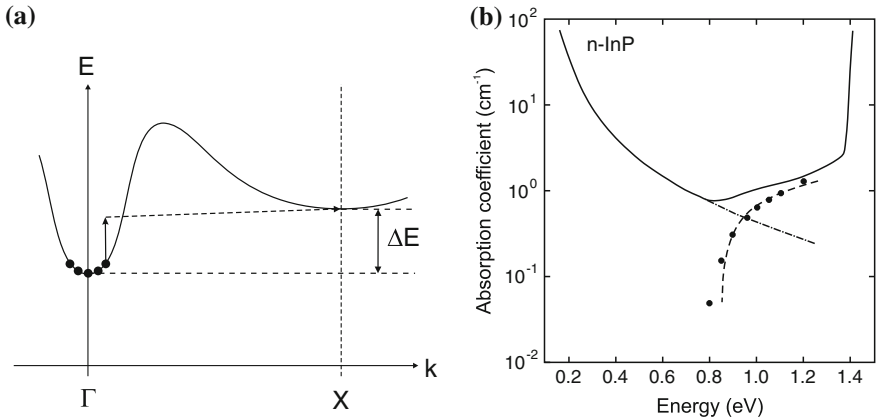


Fig. 9.44 (a) Optical absorption spectrum of GaAs:Zn with  $p = 2.7 \times 10^{17} \text{ cm}^{-3}$  at  $T = 84 \text{ K}$ . The absorption above the split-off energy  $\Delta_0$  is due to the  $hh/lh \rightarrow s-o$  process. Adapted from [811]. (b) Optical absorption coefficient of GaSb with  $p = 3.2 \times 10^{16} \text{ cm}^{-3}$ . Experimental data (solid line) and calculation of inter-valence band contribution (squares). The free carrier contribution is less than  $5 \text{ cm}^{-1}$  in the considered spectral range. Adapted from [812]

### 9.8.4 Inter-Valley Transitions

Electrons at the conduction band minimum can undergo optical transitions to the same band at a different point of the Brillouin zone. Such intervalley transition, as sketched in Fig. 9.45a, is phonon-assisted to fulfill momentum conservation and occurs around the energy difference  $\Delta E$  between the two valleys (cmp. Table 8.4).

For InP with an electron concentration of  $n = 1.65 \times 10^{18} \text{ cm}^{-3}$ , below the fundamental band edge at 1.4 eV, an additional contribution starting around 0.8–0.9 eV is found besides the free carrier absorption (Fig. 9.45b) [813]. Taking into account the filling of the bottom of the conduction band, an energy separation for the two valleys of  $\Delta E = 0.90 \pm 0.02 \text{ eV}$  was found for various values of the electron



**Fig. 9.45** (a) Schematic of inter-valley conduction band transitions involving a photon (*solid line arrow*) and a phonon (*dashed line arrow*). (b) Optical absorption coefficient of InP with  $n = 1.65 \times 10^{18} \text{ cm}^{-3}$ . Experimental data (*solid line*) and calculation of inter-valley band contribution (*dashed line*). The extrapolated free carrier contribution is shown as *dash-dotted line* and the difference of experimental absorption and extrapolated free carrier contribution as *circles*. Adapted from [813]

concentrations. This energy corresponds to the energy difference of conduction band minima at  $\Gamma$  and X in InP. The lineshape of this absorption processes can be modeled and fits well the difference of measured absorption and extrapolated free-carrier absorption spectra. Transitions to the lower minimum at L ( $\Delta E = 0.6 \text{ eV}$ ) are not observed, possibly masked by the free-carrier absorption.

### 9.8.5 Intra-Band Transitions

Phonon-assisted transitions within the lowest conduction band (not to a different valley), as indicated schematically in Fig. 9.46a for the  $\text{SnO}_2$  band structure [814], can cause absorption at photon energies below the fundamental absorption edge. Actually in  $\text{SnO}_2$ , the optical transition across the fundamental band gap is only weakly dipole-allowed and leads to small absorption coefficient below  $100 \text{ cm}^{-1}$  directly above the fundamental band gap of about 3.6 eV. The strong dipole-allowed transition with absorption coefficient around  $10^5 \text{ cm}^{-1}$  begins at about 4.3 eV and stems from electrons in a lower valence band [815]. The free-carrier absorption due to transitions within the lowest conduction band are calculated to start already at 2.8 eV (Fig. 9.46b) and thus can also impact transparency in the visible spectral range.

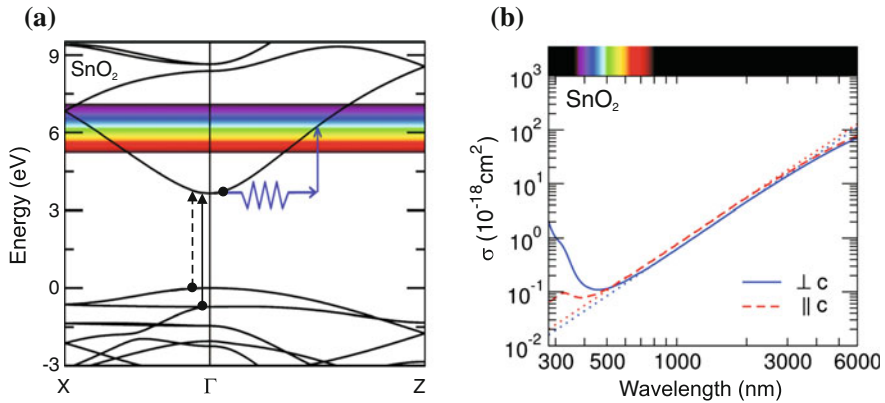


**Fig. 9.46** (a) Band structure of  $\text{SnO}_2$  and absorption processes; the transition from the topmost valence band (*dashed arrow*) is forbidden. (b) Calculated free-carrier absorption ( $\sigma = \alpha/n$ ) for  $\text{SnO}_2$ . The *solid* and *dashed* lines are results including phonon-assisted transitions for two light polarizations. The *dotted* lines are fits of the Drude model to the infrared regime. Adapted from [814]

## 9.9 Lattice Absorption

While there is no interaction of optical phonons and (infrared) light in Si and Ge due to crystal structure symmetry [816], strong effects are present for compound semiconductors. A review can be found in [817].

### 9.9.1 Dielectric Constant

The dielectric constant (with damping parameter  $\Gamma$ ) in the vicinity of the optical phonon energies is given by (cf. (5.50))

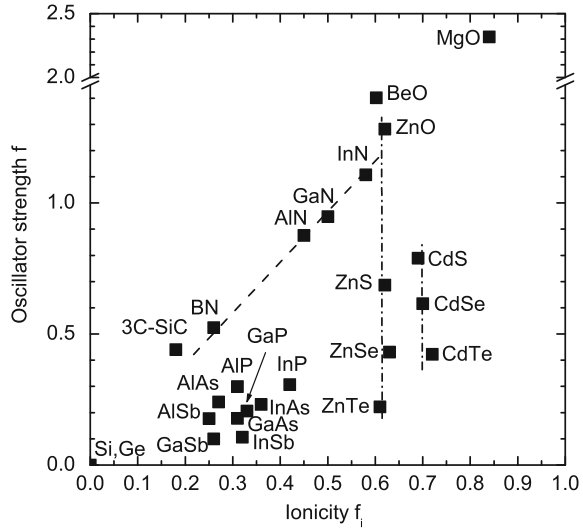
$$\epsilon(\omega) = \epsilon(\infty) \left( \frac{\omega_{\text{LO}}^2 - \omega^2 - i\omega\Gamma}{\omega_{\text{TO}}^2 - \omega^2 - i\omega\Gamma} \right). \quad (9.72)$$

The dispersion relation (without damping) can be written as

$$\epsilon(\omega) = \epsilon(\infty) + \frac{\epsilon(0) - \epsilon(\infty)}{1 - (\omega/\omega_{\text{LO}})^2} = \epsilon(\infty) \left[ 1 + \frac{f}{1 - (\omega/\omega_{\text{LO}})^2} \right]. \quad (9.73)$$

Thus the oscillator strength (compare with (D.10)) is  $f = \frac{\epsilon(0) - \epsilon(\infty)}{\epsilon(\infty)}$ . With the LST relation (5.49) the oscillator strength is

**Fig. 9.47** Lattice absorption oscillator strength  $f$  from (9.74) for various elemental, III–V and II–VI semiconductors as a function of their ionicity  $f_i$  (cf. Table 2.1). Dashed line is linear dependence on ionicity for similar (reduced) mass, dash-dotted lines are guides to the eye for similar ionicity and varying mass



$$f = \frac{\omega_{\text{LO}}^2 - \omega_{\text{TO}}^2}{\omega_{\text{TO}}^2} \approx 2 \frac{\omega_{\text{LO}} - \omega_{\text{TO}}}{\omega_{\text{TO}}}, \quad (9.74)$$

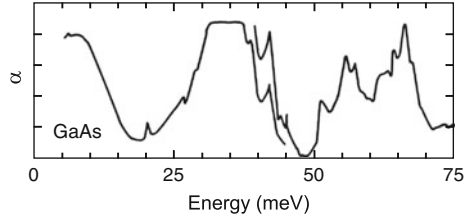
and thus proportional to the splitting  $\Delta_{\text{LT}} = \omega_{\text{LO}} - \omega_{\text{TO}}$  between the longitudinal and transverse optical phonon frequency. The approximation in (9.74) is valid for  $\Delta_{\text{LT}} \ll \omega_{\text{TO}}$ .

The oscillator strength increases with the ionicity, i.e. the electronegativity difference of the atoms in the base (Fig. 9.47). Additionally, the oscillator strength depends on the reduced mass and the high-frequency polarizability; this can be seen, e.g., for the series of the Zn compounds that all have similar ionicity. For the series of the nitrides, the mass effect is small since the reduced mass is dominated by the light N mass.

## 9.9.2 Reststrahlenbande

The absorption of electromagnetic radiation by optical phonons is governed by the dielectric function that has been derived in (9.72). For small damping, i.e.  $\Gamma \ll \Delta_{\text{LT}}$ , the dielectric constant is negative between  $\omega_{\text{TO}}$  and  $\omega_{\text{LO}}$ . From  $\epsilon_r = n_r^2 - \kappa^2$  it follows that  $\kappa^2$  is much larger than  $n_r^2$ . Therefore, the reflectance (9.17) will be close to 1. This energy range is the so-called *reststrahlenbande*. This term stems from multiple reflections in this wavelength regime that suppresses neighboring spectral regions and thus achieves a certain monochromatization in the far-infrared spectral region. Within the semiconductor the absorption is large in the reststrahlenbande (Fig. 9.48).

**Fig. 9.48** Far-infrared absorption of GaAs. In the region around 35 meV is the reststrahlenbande with high absorption due to optical phonons. Adapted from [146], based on [818]



### 9.9.3 Polaritons

The coupled propagation of phonons and electromagnetic radiation is related to the equation (without phonon damping)

$$\epsilon(\omega) = \epsilon(\infty) \left( \frac{\omega_{LO}^2 - \omega^2}{\omega_{TO}^2 - \omega^2} \right) = \frac{c^2 k^2}{\omega^2}. \tag{9.75}$$

There are two branches of propagating waves (real  $k$ ):

$$\omega^2 = \frac{1}{2} \left( \omega_{LO}^2 + \frac{c^2 k^2}{\epsilon(\infty)} \right) \pm \sqrt{\frac{1}{4} \left( \omega_{LO}^2 + \frac{c^2 k^2}{\epsilon(\infty)} \right)^2 - \left( \frac{c^2 k^2 \omega_{TO}^2}{\epsilon(\infty)} \right)^2}. \tag{9.76}$$

For  $k = 0$  we find the solutions  $\omega = \omega_{LO}$  and  $\omega = kc/\sqrt{\epsilon(0)}$ . For large  $k$  we find  $\omega = \omega_{TO}$  and  $\omega = kc/\sqrt{\epsilon(\infty)}$ . These solutions are shown in Fig. 9.49. Both branches have a phonon- and a photon-like part. The coupled state between the phonon and the photon field is called the (phonon-) polariton.

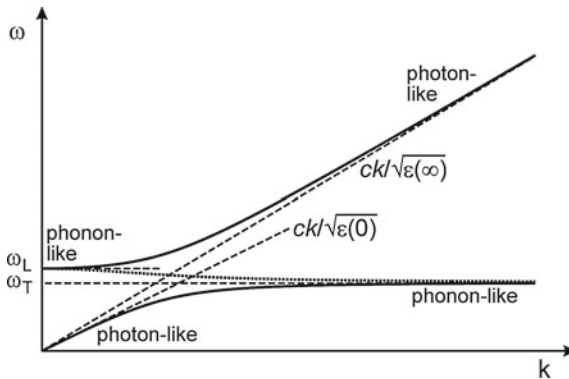


**Fig. 9.49** Dispersion of the polariton. The dotted line displays the dispersion for a purely imaginary wavevector with the absolute value  $k$

In the interval  $[\omega_{\text{TO}}, \omega_{\text{LO}}]$  the wavevector is purely imaginary, i.e.  $k = i\tilde{k}$  with real  $\tilde{k}$ . For this case there is only one solution that is also depicted in Fig. 9.49,

$$\omega^2 = \frac{1}{2} \left( \omega_{\text{LO}}^2 + \frac{c^2 \tilde{k}^2}{\epsilon(\infty)} \right) + \sqrt{\frac{1}{4} \left( \omega_{\text{LO}}^2 + \frac{c^2 \tilde{k}^2}{\epsilon(\infty)} \right)^2 + \left( \frac{c^2 \tilde{k}^2 \omega_{\text{TO}}^2}{\epsilon(\infty)} \right)^2}. \quad (9.77)$$

### 9.9.4 Phonon–Plasmon Coupling

The coupling of phonons and plasmons in the spectral region of the reststrahlenbande leads to the development of two new branches, the longitudinal phonon plasmon modes (LPP+ and LPP–), in the common dispersion. The dielectric function is

$$\epsilon(\omega) = \epsilon(\infty) \left( 1 + \frac{\omega_{\text{LO}}^2 - \omega^2}{\omega_{\text{TO}}^2 - \omega^2} - \frac{\omega_{\text{p}}^2}{\omega^2} \right). \quad (9.78)$$

For  $\epsilon(\omega) = 0$  for  $k = 0$  (coupling to photons) the two solutions  $\omega_{\text{LPP+}}$  and  $\omega_{\text{LPP-}}$  do not cross as a function of  $\omega_{\text{p}}$  (Fig. 9.50),

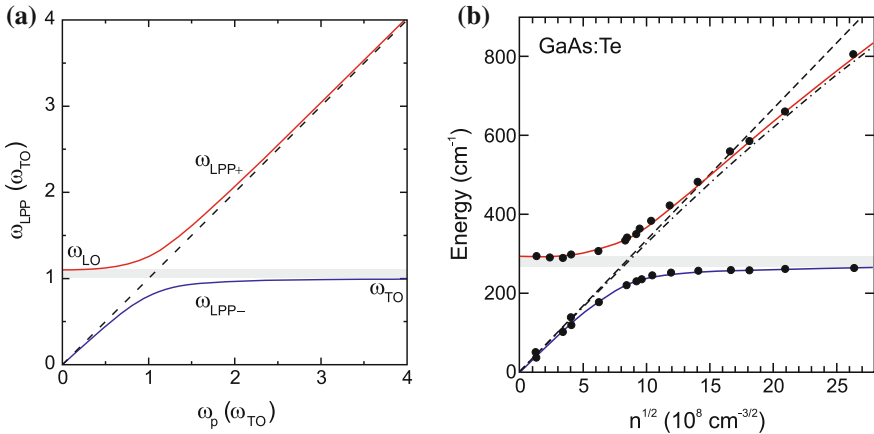


**Fig. 9.50** (a) Frequency of the coupled longitudinal-phonon plasmon (LPP) modes (lower (upper) polariton branch in blue (red)) as a function of the plasma frequency. Dashed line shows uncoupled plasmon frequency ( $\omega = \omega_{\text{p}}$ ), grey area indicates spectral region between TO and LO modes. (b) Experimental data on the polariton energies in n-type GaAs with different carrier concentration  $\omega_{\text{p}} \propto \sqrt{n m^*}$  (9.65). Dashed (dash-dotted) line is plasmon frequency  $\omega_{\text{p}}$  without (with) consideration of conduction band non-parabolicity (cf. Fig. 6.31b). Data from [805, 819]

$$\omega_{\text{LPP}\pm} = \frac{1}{2} \left[ \omega_{\text{LO}}^2 + \omega_{\text{p}}^2 \pm \sqrt{(\omega_{\text{LO}}^2 + \omega_{\text{p}}^2)^2 - 4\omega_{\text{TO}}^2 \omega_{\text{p}}^2} \right]. \quad (9.79)$$

For small plasma frequencies  $\omega_{\text{LPP}+} = \omega_{\text{LO}}$ , i.e. the optical phonons couple to the electromagnetic field without change. Also  $\omega_{\text{LPP}-} = \omega_{\text{p}}$ . For large carrier density, i.e.  $\omega_{\text{p}} \gg \omega_{\text{LO}}$ , we find  $\omega_{\text{LPP}-} = \omega_{\text{TO}}$  and  $\omega_{\text{LPP}+} = \omega_{\text{p}}$ . Thus, the carriers have effectively screened the electric field of the phonon that had led to the increase of the TO to the LO frequency.